Analysis of Protein-Protein Interactions in Live Cells: The Micro-Patterning Approach

Peter Lanzerstorfer, Andrea Steininger, Otmar Höglinger, Julian Weghuber
University of Applied Sciences Upper Austria, Wels, Austria

Daniela Borgmann, Susanne Schaller, Stephan Winkler
University of Applied Sciences Upper Austria, Hagenberg, Austria

Mario Brameshuber, Stefan Sunzenauer, Gerhard Schütz
Institute of Applied Physics, Vienna University of Technology, Austria

1 Protein-Protein-Interactions

1.1 The Relevance and Nature of Protein-Protein Interactions

Proteins are key-players that enable most biological processes in a cell, among them cell growth and proliferation, gene expression, inter and intracellular communication, cell morphology and motility. The study of protein functions is complex with many critical aspects including the expression profile, post-translational modifications, a distinct intracellular localization as well as interactions with other proteins (Golemis, 2005).

Protein-protein interactions (PPIs) occur when two or more proteins bind together. In most cases these binding processes are necessary for the biological function of the protein. The nature of PPIs can be characterized as stable or transient, and both interaction types can be strong or weak, fast or slow. The interactions of proteins that can be purified as multi-subunit complexes are defined as stable interactions. For example, hemoglobin forms a stable complex by multi-subunit interaction (Bucci *et al.*, 1965). Other well-known examples include more complicated assemblies of polypeptides, including metabolic enzymes, the DNA-replication complex or the nuclear pore complex. In many cases their activity is associated with large structures termed protein machines (Alberts & Miake-Lye, 1992).

Transient interactions are temporary in nature and usually demand special conditions that promote the interaction, e.g. changes in protein conformation or post-translational modifications. Thus, transient interactions control the majority of cellular processes, among them signaling, folding, transport, metabolic pathways or protein modification. Importantly, the study of transient interactions is much more difficult, because the factors responsible for the transient interaction have to be identified first.

PPIs are mediated by a combination of salt bridges, hydrophobic bonding and van der Waals forces at specific binding domains on the respective proteins. These domains differ in size, varying from small binding clefts of just a few peptides, e.g. the 15-residue sequence ubiquitin interacting motif (UIM) (Swanson, Kang, Stamenova, Hicke, & Radhakrishnan, 2003), to large, hundreds of amino acids spanning surfaces, e.g. the Formin Homology-2 (FH2) domain (Xu *et al.*, 2004). In general, the domain-size determines the interaction strength of the interacting proteins and the number of newly characterized PPI motifs has highly increased (Pawson & Nash, 2003; Ponting & Russell, 2002). A central player in controlling PPIs is the phosphorylation of proteins, as a post-translational modification: Many important signaling molecules such as hormones, cytokines, antigens and components of the extracellular matrix bind to membrane receptors, which then transmit signals by cytoplasmic protein tyrosine kinase (PTK) domains. Target proteins of these PTKs often show similar sequences of 50-100 amino acids although they have quite different biochemical functions (Ponting & Russell, 2002).

One of the most important and most intensely studied protein recognition domains are the Src-homology-2 (SH2), Src-homology-3 (SH3) and the pleckstrin homology (PH) domains (Haslam, Koide, & Hemmings, 1993; Pawson, 1995; Sadowski, Stone, & Pawson, 1986; Tyers *et al.*, 1988). SH2 domains bind specific phosphotyrosine residues on activated receptors, SH3 domains bind polyproline motifs and PH domains bind polyphosphoinositides, βγ-subunits of G-proteins and protein kinase C with high specificity (Pawson & Scott, 1997; Rebecchi & Scarlata, 1998). These three domains have a few common properties: first, they occur in different types of signal transduction proteins such as protein kinases, lipid kinases, protein phosphatases, phospholipases, Ras-controling proteins and transcription factors. Second, SH3 and PH domains are also involved in the mediation of signaling processes of cell movement and cellular architecture, as they can be found in cytoskeleton proteins. Third, none of these domains are

found in prokaryotes whereas all of them appear in eukaryotes except for SH2 domains, which cannot be found in yeast (Cohen, Ren, & Baltimore, 1995). Numerous SH2-containing proteins (e.g. proteins including Grb-, Nck-, STAT- and Crk-family, p56Lck) have been identified, which are mainly involved in receptor tyrosin kinase (RTK) signaling (e.g. platelet-derived growth factor receptor, PDGFR; epidermal growth factor receptor, EGFR; fibroblast growth factor receptor, FBGFR) (Cohen, *et al.*, 1995; Pawson, Gish, & Nash, 2001). The SH3 domain is part of proteins including tyrosine kinases, phospholipase C-γ (PLC-γ), PI3K, GTPase-activating protein, the cell proliferation proteins Crk and Grb2 and the cytoskeletal proteins spectrin, myosin 1 and actin-binding protein (Mayer, 2001). Pleckstrin homology (PH) motifs can be found in many different eukaryotic proteins. Important protein families which contain PH domains are Ser/Thr protein kinases, insulin receptor substrates (IRS), tyrosin protein kinases, regulators of small G-proteins (e.g. Ras-GRF), guanine nucleotide exchange proteins (e.g. vav, dbl, SoS) and GTPase activation proteins like rasGAP and BEM2/IPL2 (Rebecchi & Scarlata, 1998).
PPIs can lead to numerous different measurable effects (Phizicky & Fields, 1995). These include:

i) the alteration of the kinetic properties (e.g. altered binding of substrates),

ii) the formation of new binding sites,

iii) the inactivation of the protein,

iv) the change of the specificity of a protein for its substrate or

v) the induction of substrate channeling.

These diverse effects point out the importance of PPIs and within the last 20 years it became apparent that PPIs are much more widespread than once suspected. It is necessary to fully understand their significance in the cell and therefore the identification of PPIs, their extent to which they take place, as well as their consequences appeare vitally important. With the introduction of *Proteomics*, the large-scale study of proteins, particularly their structures and functions, in the late 90ies (James, 1997), identification and characterization of PPIs became even more relevant.

Recently, a discipline at the intersection of biology and bioinformatics that studies the interactions and also the consequences of interactions between proteins and other molecules within a cell (termed *Interactomics*), has attracted more and more attention. Interactomics differs from cellular proteomics in that it characterizes the interactions between all molecules within the cell, being non-restricted to the analysis of the interaction between proteins only. Currently, the organism whose interactome is best described is the one of *Saccharomyces cervisisae*. Over 90% of its proteins have been screened and their interactions characterized (Krogan *et al.*, 2006; Uetz *et al.*, 2000). However, further efforts in the work on PPIs will be necessary to explore also interactomes of proteins involved in biological processes and molecular functions of higher eukaryotic cells. In this regard the analysis of PPIs will play a central role to achieve these objectives.

1.2 Methods to Study Protein-Protein-Interactions

1.2.1 Overview

During the last 15 years there has been an enormous development within the field of proteomics. Different innovative assays for the identification and characterization of PPIs have been introduced. In many cases the technological development is based on great advances in mass spectrometry (MS). Generally, the identification of proteins using this technique has become a more and more simple task, enabling the

purification and analysis in the mass spectrometer in a direct fashion (Sharon & Robinson, 2007; Synowsky, van den Heuvel, Mohammed, Pijnappel, & Heck, 2006). These studies indicated that MS techniques can be used to characterize protein-assemblies. Accordingly, MS was combined with other PPI screens on a large scale to identify PPIs on a genome-wide scale (Ewing *et al.*, 2007; Stelzl *et al.*, 2005). However, the rate of false positives (30-60%) and false negatives (between 40-80%) appear enormously high and only a very limited number of found interactions is supported by more than one assay (von Mering *et al.*, 2002). This obvious fact cannot be explained only by the application of many different assays. Thus the experimental validation of PPIs using different methods or the usage of assays that result in a limited number of false positives and negatives is crucial.

An important issue is the application of *in-vitro* techniques in comparison to applications in living cells. The first ones take place outside of a cellular context and can lead to artifacts that are not reflective of the native cell state. Additionally, it has become clear that PPI networks are regulated spatially (Teis, Wunderlich, & Huber, 2002). This spatial information is of course lost when the cellular environment is destroyed and therefore *in-vitro* derived PPI maps lack information of the subcellular localization as well as the cellular state. Thus the development of methods capable of detecting PPIs under native conditions is a central point.

1.2.2 *In vitro* Applications

The most commonly used approach to identify PPIs is based on affinity purification of interaction partners of a bait protein. Routinely this is done by co-immunoprecipitation – Co-IP – (Barrios-Rodiles *et al.*, 2005). In doing so an antibody that targets a known protein that is a putative member of a protein complex is selected. In many cases it is possible to pull the whole complex out of solution ("pull-down") rendering the identification of unknown complex members possible. This procedure only works when the proteins involved in the complex bind tightly to each other. In addition, successful application of Co-IP demands for several rounds of precipitation using different antibodies as well as different complex partners. During the assay the proteins are kept in their native state and – unless transfection is used – also at their native concentration. However, disadvantages of Co-IP include:

i) the detection of stable interactions only,

ii) the mixing of compartments during cell lysis whereby interacting proteins might not be in the same cellular compartment,

iii) the requirement of antibodies and

iv) the missing certainty that detected interactions are really direct ones.

A powerful strategy is to modify the bait-protein with a tag. For example Tandem Affinity Purification (TAP) involves the establishment of a fusion protein including a short tag on one end (Puig *et al.*, 2001). The fusion protein binds to a bead-coated antibody: the TAP tag is cleaved enzymatically and finally binds to further beads. This procedure allows for specific purification of the prey proteins, which can be subsequently analyzed by mass spectrometry. Additionally successive purification rounds reduce the number of contaminants. However, it is cogitable that the tag affects protein expression levels or influences the binding to the interaction partner, which is a general problem of such methods. Furthermore the tag may also not be sufficiently exposed to the affinity beads and thus correct interaction partners would not be identified. Despite these drawbacks the TAP-tag approach was successfully implemented and – in combination with mass spectrometry – resulted e.g. in a large-scale analysis of yeast multiprotein com-

plexes (Gavin *et al.*, 2002). Other tag-strategies include i) affinity tags like the chitin binding protein (CBP), the maltose bind protein (MBP) and the glutathione-S-transferase (GST) and ii) short peptide tags, e.g. the HA-, FLAG- or His-tag.

A widely used *in-vitro* method based on a tag-strategy is the Strep-tag system. This tag is a synthetic peptide consisting of eight amino acids and exhibits affinity towards an engineered streptavidin (Strep-Tactin) (Schmidt & Skerra, 2007). It can be easily fused to recombinant proteins just like other short-affinity tags. However, there are several advantages of using the Strep-tag system including its small size and the fact that it is biochemically inert. In addition the purification procedure can be kept under physiological conditions and isolated proteins are bioactive and display a high purity. This allows for the purification of intact protein complexes and thus renders the study of PPIs possible (Junttila, Saarinen, Schmidt, Kast, & Westermarck, 2005).

Generally, if applying tag-based technologies, researchers should be aware of the following matters of fact:

i) in some cases the tag may cause problems, thus both N- and C-terminally tagged proteins should be tested.

ii) the tag can be buried inside a complex, which precludes the detection e.g. on an affinity column.

iii) the tag might influence the affinity between the protein-complex members.

iv) frequently, the tag affects the localization of the bait protein. For example N-terminal fusions of certain proteins preclude their correct membrane localization. In such a way N-terminal fusions of the palmitoylated and myristoylated tyrosine kinase Lck are problematic (Yasuda *et al*., 2000).

A classical method to detect PPIs is chemical crosslinking. Therefore reagents such as formaldehyde, imidoesters or hydroxysuccinimide-esters are used to crosslink proteins via lysine residues. The basic principle is that two proteins that are in close proximity – but do not form a stable complex – can be linked by chemical crosslinkers. By varying the size of the crosslinker – mainly by choosing reagents with different spacer lengths – different complexes can be successfully crosslinked. However, these substances are generally much less selective and allow for crosslinking independent of the binding domain. The main advantage of the crosslinking methods is that also transient or weak PPIs may be detected. For example a mitochondrial magnesium-channel was reported to act as a pentamer based on cross-linking experiments (Kolisek *et al.*, 2003). This finding could be later confirmed by X-ray scattering of channel crystals (Lunin *et al.*, 2006). Furthermore, crosslinking can be combined with other approaches (Tagwerker *et al.*, 2006). An interesting advancement of the crosslinking approach was the introduction of photo-crosslinking to stabilize interactions prior to cell lysis (Suchanek, Radzikowska, & Thiele, 2005). In this assay cells are grown with photoreactive amino acid analogs, which are incorporated into proteins. Exposure to UV light activates the analogs which then bind to interacting proteins that are within close vicinity. A human signaling protein was successfully photo-crosslinked by a similar approach (Hino *et al.*, 2005).

1.2.3 Live Cell Applications

Several approaches were developed for the analysis of PPIs in a live cell context and also sometimes combined with *in-vitro* techniques. An important approach is the linkage of two proteins of interests to non-functional protein-fragments, called protein-fragment complementation assays (PCAs).

Upon interaction bait and prey complement each other to reconstitute a functional protein, which is finally detected. A prominent representative of this strategy is the two-hybrid system Y2H (Fields & Song, 1989): a transcription factor is split into two separate fragments, termed binding domain (BD) and activating domain (AD), and activates a downstream reporter gene by binding onto an upstream activation sequence. Although adapted to address alternative questions (e.g. the detection of protein-DNA interactions and the use of bacteria instead of yeast), the basic principle has not been changed (Hurt, Thibodeau, Hirsh, Pabo, & Joung, 2003). The Y2H method offers the advantages of being low-tech, providing an important first hint for the identification of interaction partners and being scalable, and furthermore it can be automated. However, there are several weaknesses, with the high number of false positive and negative hits being the most important one (Deane, Salwinski, Xenarios, & Eisenberg, 2002). The reason for these high error rates include

i) the drawbacks of the necessary protein fusion,

ii) in many cases overexpression of the fusion proteins leads to unnatural protein concentrations,

iii) the missing of interactions in case of proteins that cannot be translocated into the nucleus and

iv) the coexistence of bait and prey in yeast only, where temporal or spatial segregation is lacking compared to other eukaryotic cells.

Due to combined effects of all error sources Y2H results must be carefully validated and confirmed by high confidence assays. A major disadvantage that has not been mentioned yet is the impracticality to study PPIs between integral membrane proteins with Y2H. To overcome this limitation the split-ubiquitin system has been implemented. In this system the membrane localized bait and prey proteins are fused to two different ubiquitin moieties (*Cub* and *Nub*). Upon interaction the reconstituted split-ubiquitin molecule indirectly leads to the induction of reporter genes (Stagljar, Korostensky, Johnsson, & te Heesen, 1998).

Further PCAs include so-called bimolecular fluorescence complementation assays (BiFC). In that case fluorescent proteins are reconstituted which means that the interaction of bait and prey brings the fluorescent fragments within proximity and leads to a fluorescent signal (Kerppola, 2006). For example yellow fluorescent protein (YFP) was successfully splitted and reconstituted to prove the interaction of transcription factors (Hu, Chinenov, & Kerppola, 2002). The strengths of this approach include the possibility of direct visualization and the high sensitivity leading to the detection also of weak interactions with spatial resolution. To carry out the experiments only a simple fluorescence microscope is needed. However, the method suffers from the limitation being unable to provide real-time detection of PPIs: the fluorescent signal takes some time to be produced after initial interaction of bait and prey in the order of hours. Moreover, the reconstitution of the fluorochrome is irreversible in most cases and – similar to other protein-fusion strategies – the protein structure of bait and prey might be affected by the fluorescent protein fragments.

A widely used method to study PPIs in living cells utilizes the energy transfer between a donor and an acceptor dye also known as Förster resonant energy transfer (FRET) (Förster, 1948). The donor chromophore in its excited state transfers energy to the acceptor chromophore through nonradiative dipole-dipole coupling, when donor and acceptor are within close proximity (1- 10 nm). The efficiency of the energy transfer is inversely proportional to the distance between donor and acceptor making FRET highly sensitive to small distances (Stryer & Haugland, 1967). There are several ways of measuring the FRET efficiency by monitoring changes in the fluorescence emitted by the donor or the acceptor. One

approach is to measure the acceptor emission intensity, which increases because of FRET from the donor to the acceptor. Another method is to determine photobleaching rates of the donor in the presence/absence of an acceptor. Finally, FRET efficiencies can also be determined from the change in the fluorescence lifetime of the donor, which decreases in the presence of the acceptor (fluorescence-lifetime imaging microscopy, FLIM). In many cases, fluorescent proteins are used as FRET pairs (Jares-Erijman & Jovin, 2003). For example, the green fluorescent protein (GFP) mutants cyan fluorescent protein (CFP) and yellow fluorescent protein (YFP) are commonly applied (Pollok & Heim, 1999). Due to the fast bleaching and low fluorescent brightness of CFP, other FRET pairs like the mCherry-GFP combination have been implemented (Shaner *et al.*, 2004). Furthermore organic, photostable dyes can be used as an alternative. Another FRET variation termed BRET has been introduced by using bioluminescent luciferase instead of CFP to produce an initial photon emission compatible to YFP. In that case external illumination is not needed to initiate the energy transfer (Pfleger & Eidne, 2006). The FRET technique offers the possibility to analyze and also quantify PPIs in living cells. However, the interpretation of gained results is complicated, and many control experiments appear obligatory. Additionally, FRET measurements can be pH sensitive and only work if the fluorophores are in a correct orientation. The implementation of FLIM boosted the FRET technique, but for this approach expensive secondary equipment is needed.

Further methods to study PPIs in live cells include confocal microscopy, fluorescence cross-correlation (FCS) analysis of interacting proteins in time or space (Digman, Wiseman, Choi, Horwitz, & Gratton, 2009; Schwille, Meyer-Almes, & Rigler, 1997) as well as single molecule microscopy (Ruprecht, 2010). Analysis of PPIs by confocal microscopy has been routinely performed for many years. However, it is not a quantitative method and generated data have to be validated with caution, mainly due to the fact that the approach does not prove interactions, but in a best case only visualizes co-localization of proteins. Data from FCS and single molecule microscopy experiments can be quantified, however, the analysis is highly complicated and time-consuming.

Finally, some non-spectroscopic methods can be used to study PPIs in live cells. For example the proximity ligation assay (PLA) uses short DNA-strand based probes that bind DNA-labeled antibodies (Soderberg *et al.*, 2006). When the PLA probes are in close proximity the DNA-strands interact in the presence of added circle-forming oligonucleotides. After enzymatic ligation these oligonucleotides are amplificated and highlighted by a fluorophore on a complimentary nucleotide. The readout can be performed by a fluorescent microscope on a single cell level as well as a suitable fluorescence reader. Another non-spectroscopic method is based on the co-immobilization of surface bound membrane proteins and their mobile ligands. By combining this approach with fluorescence recovery after photobleaching (FRAP) measurements, the oligomerization state of membrane receptors could be analyzed (Dorsch, Klotz, Engelhardt, Lohse, & Bunemann, 2009).

Taken together PPIs can be detected by numerous different approaches which each exhibit pros and cons. An important issue in this regard is the possibility to quantify the results. On the one hand methods including the Y2H screen are rather indirect and thus hardly quantitative. On the other hand quantitative approaches are available, but those are difficult to extend to high throughput. A novel approach which combines the possibility to extract quantitative information with high throughput capabilities is based on micro-structured surfaces in combination with fluorescence microscopy – the μ-patterning technique.

2 The µ-patterning assay

2.1 Overview

The µ-patterning assay is based on the finding that membrane proteins can be forced into specific patterns within the plasma membrane of live cells. By the use of microstructured glass surfaces with a bound ligand to the membrane protein of interest, this protein could be enriched in certain areas. In this way studies addressing cell adhesion, T-cell activation or the composition of signaling complexes could be performed (Cavalcanti-Adam *et al.*, 2006; Mossman, Campi, Groves, & Dustin, 2005; Wu, Holowka, Craighead, & Baird, 2004).

In order to identify and quantify interactions between a fluorophore-labeled protein (prey) and a membrane protein (bait), we have extended the approaches mentioned before (Brameshuber, 2009; Schwarzenbacher *et al.*, 2008; Weghuber, Brameshuber, *et al.*, 2010; Weghuber, Sunzenauer, Brameshuber, *et al.*, 2010). Figure 1 shows the principle of the method: A specific ligand to the exoplasmic domain of the bait is arranged in micropatterns on a glass surface; an example for such a ligand may be an antibody. The intermediate gaps are passivated with BSA. When cells expressing the bait are plated on such surfaces, the bait follows the antibody patterns. To address bait-prey interactions, the lateral distribution of fluorescently tagged prey is analyzed and compared with the antibody/BSA micropatterns. Interaction leads to pronounced co-patterning, whereas no interaction yields homogeneous prey-distribution.

The exclusive bait rearrangement is induced by specific, biotinylated ligands. For that the usage of antibodies appears straightforward. However, other ligands including biotinylated hormons, toxins or purified proteins can be applied. The read-out is performed on an epifluorescence microscope operated in total internal reflection (TIR) configuration, a microscopy technique which effectively reduces contributions from prey molecules distributed throughout the cytosol (Axelrod, 2003). An imaging resolution of at least 1 µm is required to resolve the micropatterns. Scanning capability including a focus-hold system increases the efficiency of the approach and enables the user to gain information from many cells within a short time.

As a cellular system adherent cell lines that attach tightly to the µ-biochip are preferential. Limitations are as follows the i) accessibility of the bait protein to the immobilized capture ligand and ii) the fluorescent labeling of the prey protein (e.g. genetic fusions with fluorescent proteins or tags that enable the binding of fluorophores (Regoes & Hehl, 2005)).

As indicated in Figure 2 the production of the microstructured surface is utilized by microcontact printing (Kane, Takayama, Ostuni, Ingber, & Whitesides, 1999). Fluorescent BSA is transferred to a reactive glass-surface using a microstructured PDMS stamp and the gaps are filled with streptavidin. Afterwards, the surface is functionalized using biotinylated anti-bait ligands.

As already mentioned the µ-patterning approach is a quantitative method. The interaction strength of bait and prey proteins can be quantified by the degree of prey-redistribution to bait-enriched regions (Figure 1). For that reason the fluorescence intensity inside and outside the pattern (defined as F^+ and F^-, respectively; see Figure 3) is determined and, by subtracting the global background F_{bg} (i.e. regions on the µ-biochip where no cells grow), the contrast C is computed as defined by $C=(F^+ - F^-)/(F^+ - F_{bg})$. This calculation is performed with numerous patterns from different cells (ideally min. n=100) and the results are plotted in a density plot displaying the contrast as well as the fluorescent brightness.

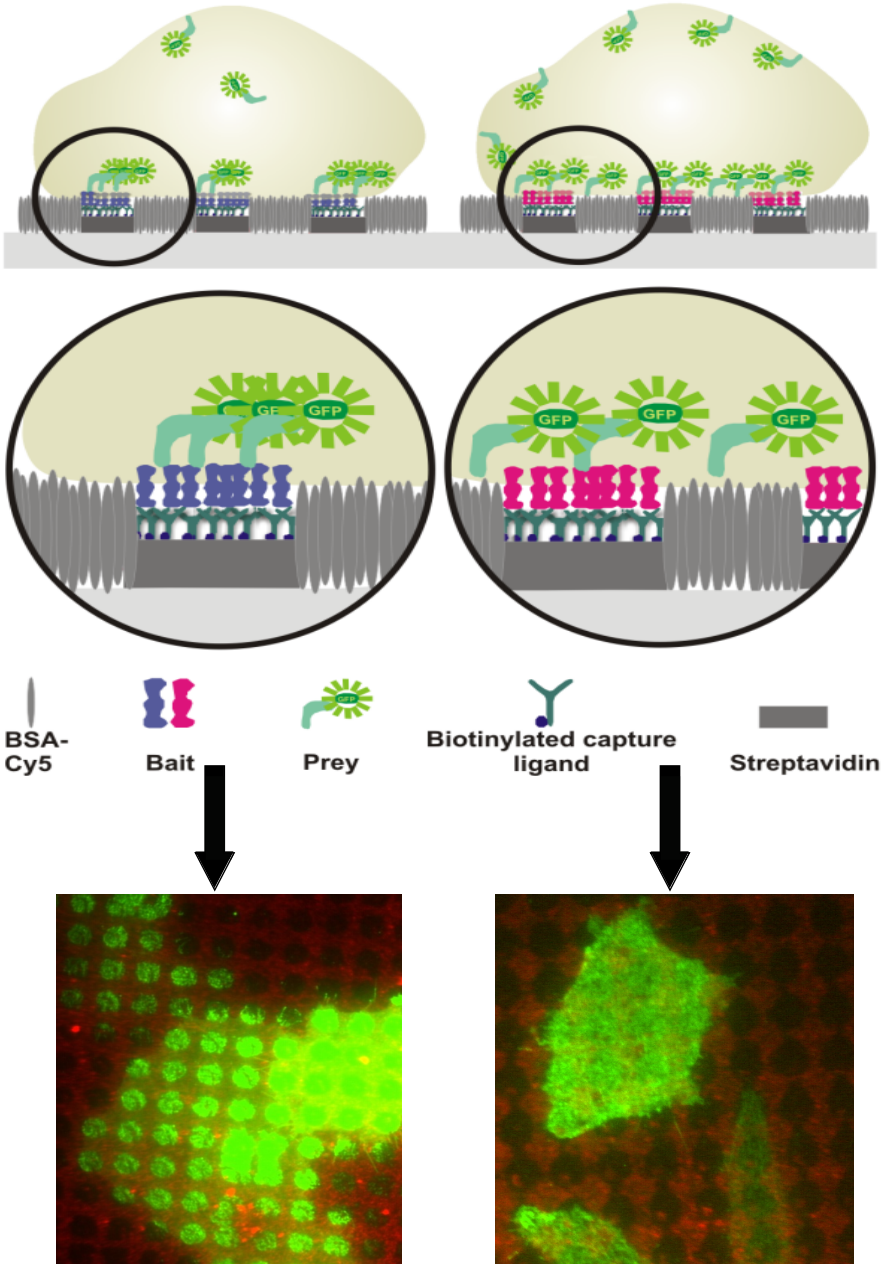

Figure 1: Schematic illustration of the µ-patterning assay. Grids of BSA-Cy5 are printed on functionalized glass coverslips, and interspaces are filled with streptavidin and biotinylated monoclonal ligands (antibodies) against the membrane protein bait. In cells grown on such µ-biochips, the bait will be arranged in the plasma membrane according to the antibody micropattern. Interactions with a second fluorescently-labeled protein (prey) induce redistribution of the prey protein to bait-patterns (left), whereas the distribution of the prey appears homogenous if there is no interaction with the bait (right). Adapted from (Schwarzenbacher, *et al.*, 2008).

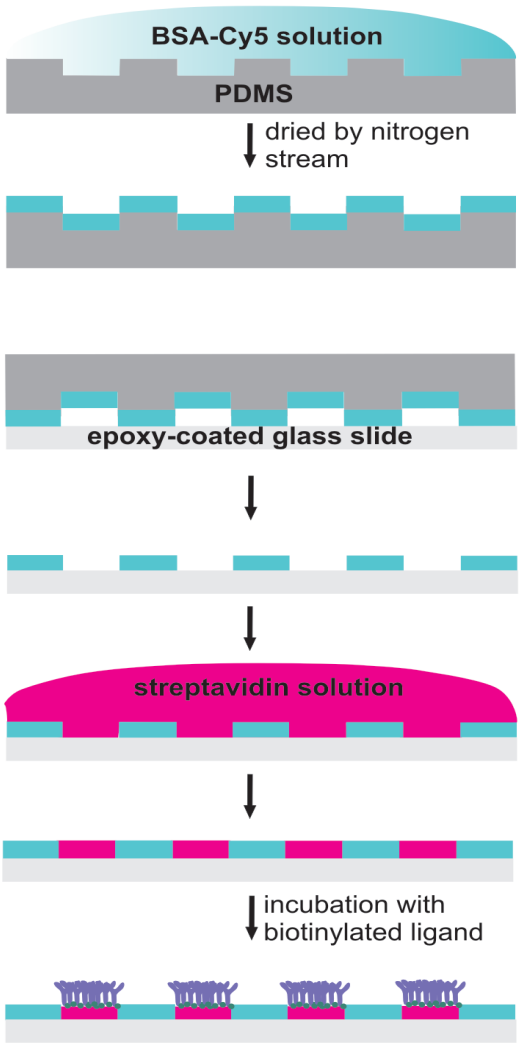

Figure 2: Microcontact-printing for producing structured surfaces. The PDMS stamp is incubated with BSA-Cy5 solution, dried, and put on a reactive glass surface. After removal of the stamp, the surface is incubated with streptavidin solution, washed, and finally incubated with biotinylated ligand. Adapted from (Weghuber, Brameshuber, *et al.*, 2010).

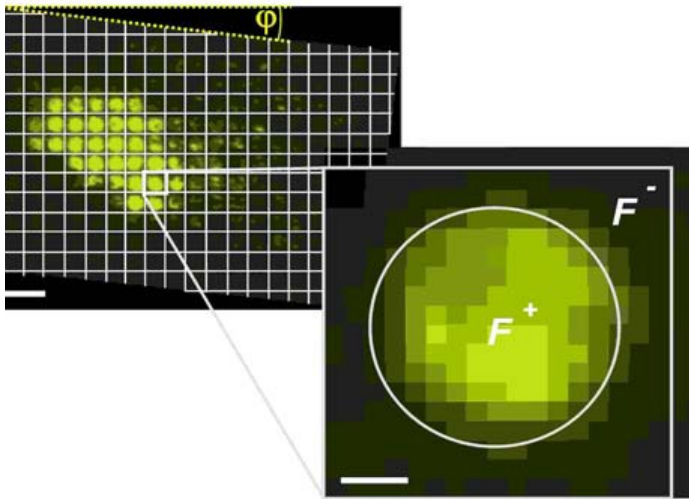

Figure 3: Contrast calculation to determine interaction strength of bait and prey. An automatic gridding algorithm to calculate the grid-size and the rotation angle φ of the image was used. The grid subdivides the total image into adjacent squares, which were quantified according to the average specific signal within a central circle (F^+) and the unspecific background outside this circle (F^-). Reproduced from (Schwarzenbacher, *et al.*, 2008).

2.2 Successful Applications of the µ-patterning Approach

In a first report the µ-patterning assay was used to characterize the interaction between human CD4, the major co-receptor in T-cell activation, and human Lck, a protein tyrosine kinase essential for early T-cell signaling (Brameshuber, 2009; Schwarzenbacher, *et al.*, 2008). Stable CD4-Lck association is regarded as the basis for Lck recruitment to the immunological synapse, the crucial site for initiation of T-cell signaling (Q. J. Li *et al.,* 2004). In this study, the interaction of these two proteins could be verified. Furthermore, multiple Lck domains contributing to CD4 binding with varying strength were found. A main finding of this report was that the interaction of CD4 and Lck could be modified by the addition of a drug (a chelator, which has been reported to disrupt the CD4-Lck interaction) to the live cell. As shown in Figure 4 the distribution of Lck-YFP followed clearly the immobilized CD4 clusters. Upon addition of the chelator the degree of prey co-patterning was remarkably reduced.

In further experiments the ability of the µ-patterning approach to detect the redistribution of other membrane proteins (e.g. CD71 – the human transferrin receptor) was confirmed (Weghuber, Brameshuber, *et al.*, 2010).

Another study was dealing with the kinetics of bait and prey redistribution after seeding the cells on the µ-biochip (Weghuber, Sunzenauer, Plochberger, *et al.*, 2010). Fast rearrangement within minutes after first contact with the surface and stable interactions of bait and prey within the first hours after cell seeding were found. For example the redistribution of GPI-GFP on anti-GFP antibody coated µ-biochips was recorded at different time points. As shown in Figure 5 the cells were able to expand or migrate on the surface without affecting the calculated overall contrast of the patterns of all analyzed cells. However, the contrast of bait patterns within a single cell varied remarkably, indicating that the bait can be released from and recaptured on the µ-patterns.

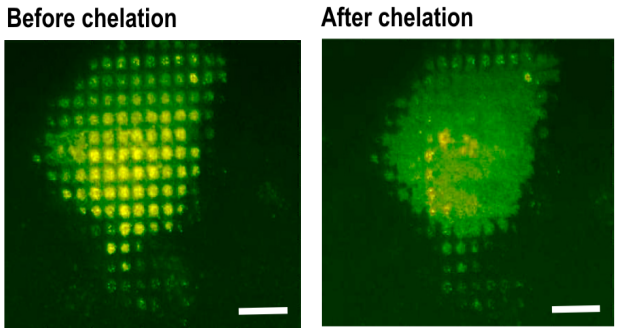

Figure 4: µ-patterning experiments for characterizing the interaction between CD4 and Lck. Influence of chelator treatment on CD4-Lck binding. T24 cells cotransfected with CD4 and Lck-YFP were plated on CD4-antibody µ-biochips in the absence (left) or presence (presence) of a chelator, which is known to disrupt the interaction of these proteins. Scale bars 20 µm. Adapted from (Schwarzenbacher, *et al.*, 2008).

An important part of the same report analyzed the detection of indirect PPIs. For that purpose the interaction of GPI-GFP with the GPI-anchored protein CD59 was determined. GPI-anchored proteins have been reported to partition into lipid rafts, nanometer-sized lipid domains in the plasma membrane (Pike, 2006). Choosing CD59 as bait and GPI-GFP as prey the analysis was restricted to indirect interaction mediated by the lipid environment. Indeed, the µ-patterning approach could approve the interaction of the lipid raft localized proteins GPI-GFP and CD59 in a live cell context (Weghuber, Sunzenauer, Plochberger, *et al.,* 2010).

Recently, Alexander and co-workers used the µ-patterning approach to demonstrate the interaction between the urokinase receptor (µPAR) and integrins in vascular endothelial growth factor (VEGF)-stimulated endothelial cells (Alexander *et al.*, 2012). The GPI-anchored protein µPAR is a specific receptor for the serine protease urokinase plasminogen activator (µPA), contributes to the extracellular matrix and regulates endothelial cell survival (Koolwijk *et al*., 2001; Prager *et al.*, 2009). In this study an antibody to the β1-integrin subunit was used to detect interaction with the µPAR protein: In unstimulated cells µPAR was distributed homogenously, while VEGF stimulation lead to redistribution to β1-integrin enriched regions (see Figure 6). Accordingly, the calculated mean contrast was 0.35 for stimulated and 0.07 for resting cells. If an activating antibody against the β1-subunit was used to redistribute the bait protein, no interaction of µPAR and β1-integrins could be detected.

The study analyzing the interaction of β1-integrins and the µPAR protein is especially interesting from a technical view: Instead of using a genetically engineered fluorescent fusion protein, a fluorescently labeled antibody was chosen to stain fixed cells. The successful antibody based prey labeling highlights the versatility of the µ-patterning approach.

Finally, a recent study addressed the quantitative characterization of the equilibrium binding between a bait and a prey protein using the µ-patterning assay combined with single molecule tools (Sunzenauer *et al.*, 2012). In this report the authors could show that saturation binding curves can be obtained, which enable the calculation of dissociation constants. Therefore, as a test system, the interaction between a primary antibody on the µ-biochip surface and a fluorescent secondary antibody in solution was analyzed. The binding curve was recorded with increasing concentrations of the secondary antibody.

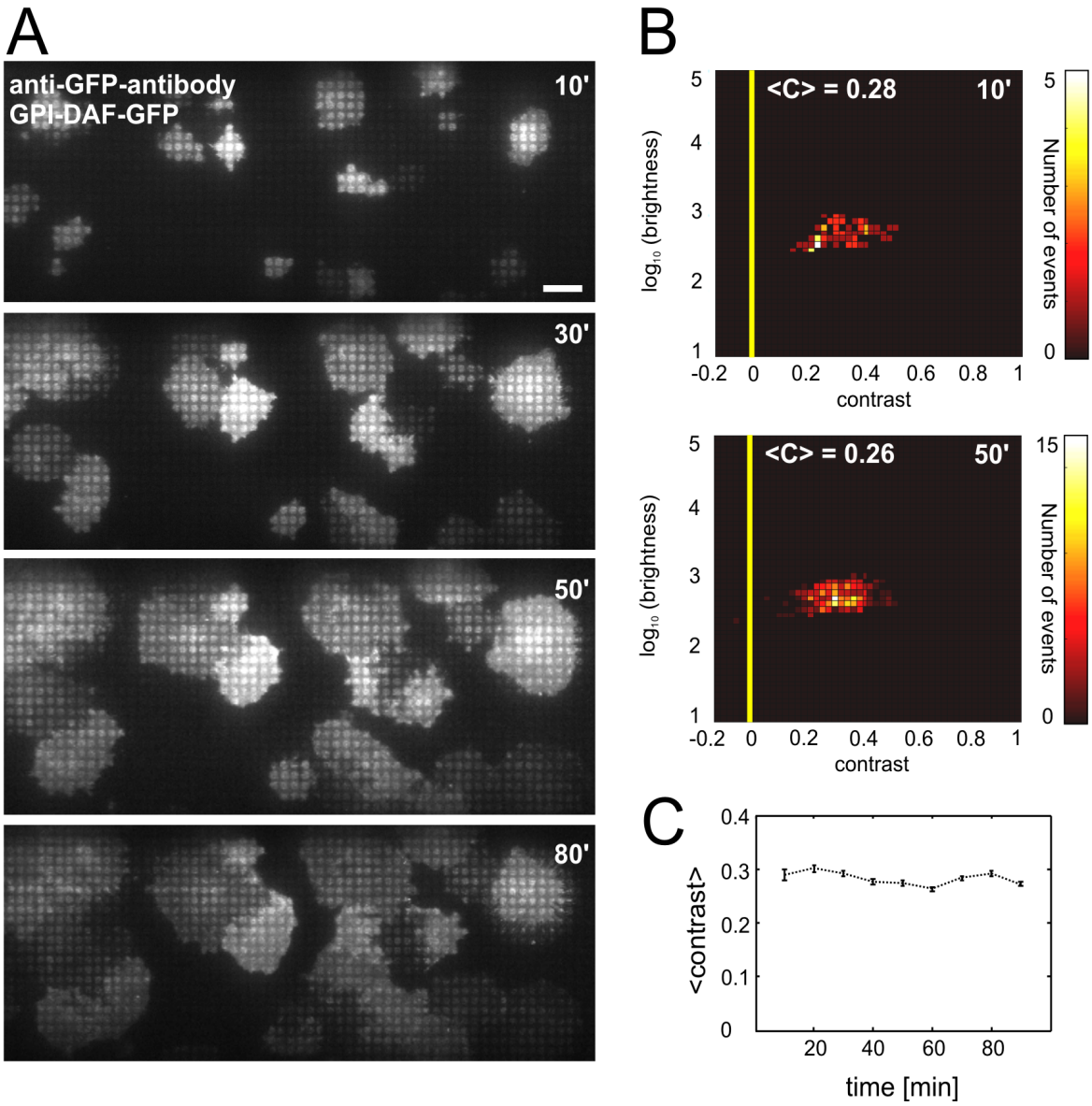

Figure 5: Temporal resolution of bait redistribution. (A) T24 cells expressing GPI-DAF-GFP were seeded on a micro-biochip coated with anti-GFP-antibody and scanned 10, 30, 50 and 80 minutes after seeding. Scale bars, 20 µm. (B) Statistical analysis of all cells in the scanning-area (after 10 and 50 minutes) is shown in color density plots for the fluorescence brightness F and mean contrast <C>. (C) Mean contrast <C> of GPI-DAF-GFP versus time after seeding the cells. Images reproduced from (Weghuber, Sunzenauer, Plochberger, *et al.*, 2010).

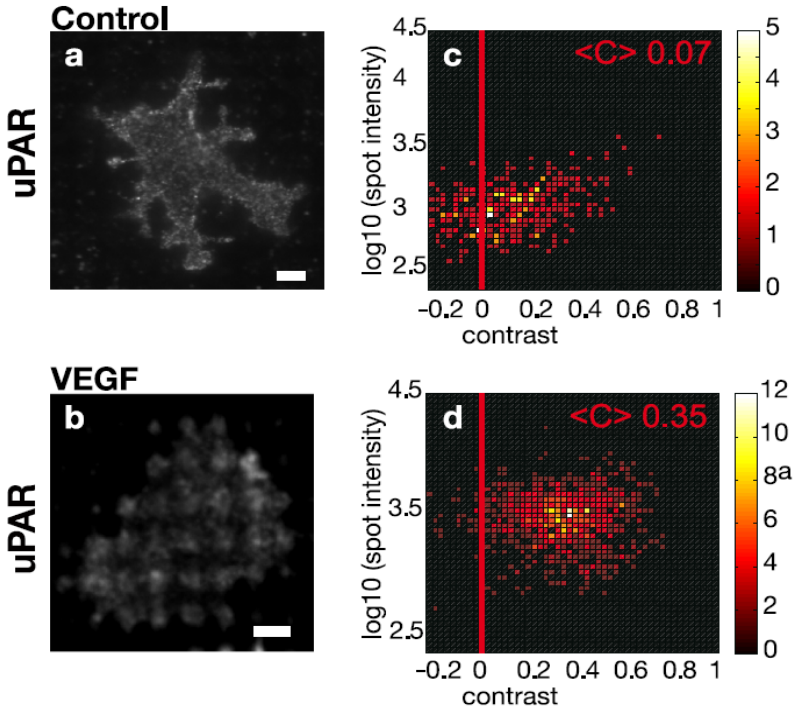

Figure 6: Interaction of μPAR and β1-integrin in endothelial cells determined by μ-patterning experiments. Cells were grown on anti-β1-integrin coated μ-biochips, fixed and immunostained with a fluorescent anti-μPAR antibody. Upper row: without VEGF induction. Lower row: with VEGF stimulation (50 ng/ml for 60 min). Statistical analysis of 64 cells is shown in color density plots for the fluorescence brightness F and mean contrast <C>. Reproduced from (Alexander, et al., 2012).

Importantly, the readout could be done with standard fluorescence microscopy without the need for TIR excitation. Furthermore, in living cells the interaction between CD4 and Lck fused with monomeric GFP was studied. In this case natural fluctuations of Lck-mGFP expression levels between different cells were used to record the binding curve. After characterizing the quality of the bait micropatterns induced by the CD4 antibody using YFP-labeled CD4, the interaction of Lck-GFP and unlabeled CD4 was determined. Due to the fact that the interaction was not saturable even in cells with highest Lck expression levels, the determination of equilibrium constants could not be determined. However, combination with single molecule microscopy indicated the recruitment of approximately 9 Lck molecules per CD4 co-receptor (Sunzenauer, et al., 2012). In conclusion, the μ-patterning technique might serve as a valuable tool to quantify equilibrium constants of bait and prey proteins *in-vitro* and living cells.

3 New Technical Developments

3.1 PDMS Master and Photomask

To meet the requirements of a well defined microstructured surface for conducting the μ-patterning experiments, a PDMS-master disc that based on a new photomask was purchased (Figure 7 A and B, re-

spectively). The new PDMS-master contains about 80 µ-structured areas with an increased size of 5 x 5 mm. This ensures that the printed BSA grid completely covers the size of a hybridization chamber in which the cells grow, thus optimizing the number of cells that can be finally analyzed in a single experiment. The µ-structured patterns (3 x 3 µm in size with a distance of 3 µm) differ from each other and appear as squares or rather as circles (Figure 7 C and D, respectively). This finding may influence the final calculation of the contrast and points out the importance of having a flexible contrast calculation program that accounts for F^+ and F^- regions of varying size or shape.

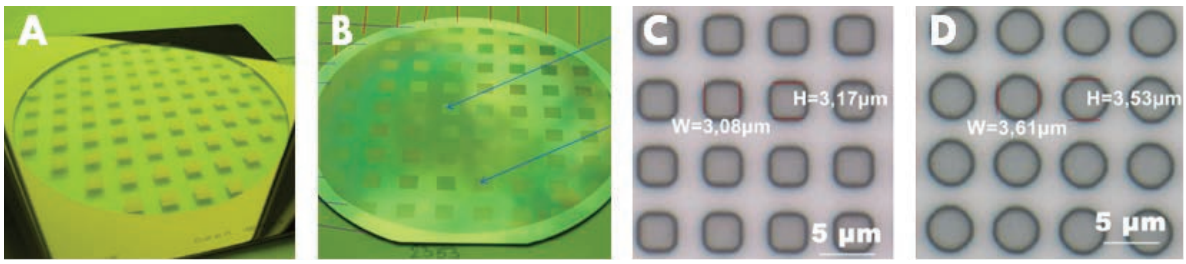

Figure 7: (A) Photomask for the PDMS-master production. (B) Respective PDMS-master. (C/D) Enlarged view of different µ-structured regions (marked by the blue arrows in (B)): the size of the PDMS-patterns is 3 x 3 µm and the distance between the patterns is 3 µm as well.

3.2 Functionalized Glass slides

In its original experimental setup the µ-patterning assay was conducted on self-made epoxysilane-coated glass slides (Schwarzenbacher, *et al.*, 2008). Despite the sufficient quality of the functionalized glass slides in many cases, we recognized a rather poor homogeneity and too low reactivity of the surface coating in some experiments. To overcome this problem we tested different commercially available glass slide coatings (Xenobind™ Aldehyde slide, Schott Nexterion® Slide E (epoxysilane), Schott Nexterion® Slide P (N-hydroxysuccinimide, NHS), Xenoprobe™ Streptavidin slide) and tested their applicability for the µ-patterning assay.

In this regard we tested the cell adhesion performance, the BSA-Cy5 printing efficiency and the reactivity of the surface coating for biotinylated ligands (Figure 8). We grew T24 cells stably expressing GPI-anchored GFP (GPI-GFP), which is a probe localized to the outer plasma membrane leaflet (Weghuber, Sunzenauer, Plochberger, et al., 2010), on anti-GFP antibody functionalized glass slides and analyzed them three hours after cell seeding. Cells attached well on all tested surfaces (Figure 8 A1-D1) with the exception of the Schott Nexterion® P slides (NHS). In that case cells did not attach at all, as indicated in Figure 8 B1. In spite of the poor cell morphology and imperfect surface adhesion, some high contrast µ-patterns of cells growing on BSA grids of perfect quality (Figure 8 B2-3) were detected, indicating redistribution of the GPI-GFP probe to anti-GFP antibody positive regions. However, the interaction was lost about 5 hours after cell seeding due to complete lack of cell adhesions. The NHS-coated glass slides are frequently used for conducting antibody microarrays to study PPIs (Blackburn & Shoko, 2011; Blackburn, Shoko, & Beeton-Kempen, 2012), but they do not seem to be the appropriate choice for live cell µ-patterning applications.

With Xenobind™ Aldehyde slides the efficiency to redistribute the GPI-GFP protein varied immensely. In some cases we obtained satisfying GPI-GFP redistribution (Figure 8 A4). However, in most experiments we could not detect any patterns at all (Figure 8 A3). These findings led us to the conclusion that the reactivity to bind biotinylated ligands is not given for these slides.

Furthermore we tested the epoxysilane coated Nexterion® E slides. We mostly observed inhomogeneous BSA-Cy5 grids (Figure 8 C2) resulting in low-contrast µ-pattern images (Figure 8 C3).

The best results could be obtained by the use of Xenoprobe™ Streptavidin coated glass slides. Besides ideal cell adhesion and efficient BSA-Cy5 transfer (Figure 8 D1-2) we could observe efficient and reliable GPI-GFP redistribution to anti-GFP antibody positive regions (Figure 8 D3). In order to successfully use these streptavidin coated slides it was necessary to alter the µ-contact printing procedure: Efficient binding of BSA-Cy5 to the streptavidin surface demanded a modification of BSA-Cy5 with NHS-cap-Biotin. Additionally, the initial step of streptavidin incubation before antibody addition became redundant (also see Figure 10).

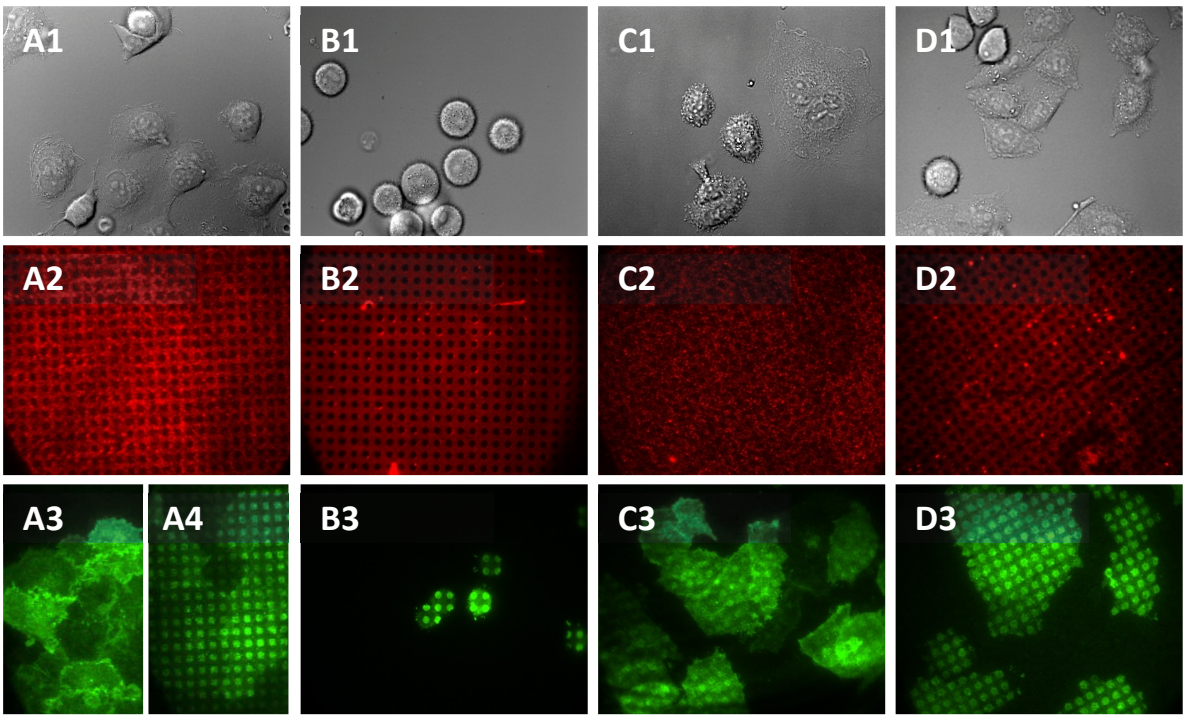

Figure 8: Comparison of the suitability of functionalized glass slides with different surface coatings for µ-patterning experiments. T24 cells expressing GPI-GFP were grown on anti-GFP antibody functionalized (A) Xenobind™ Aldehyde, (B) Schott Nexterion® Slide P (N-hydroxysuccinimide, NHS), (C) Schott Nexterion® Slide E (Epoxysilane) and (D) Xenoprobe™ streptavidin slides, respectively. **Upper row:** cell adhesion capability (DIC images). **Middle row:** TIRF image at 640 nm showing BSA-Cy5 grid. **Bottom row:** TIRF images at 488 nm indicating GPI-GFP redistribution to anti-GFP antibody positive regions.

3.3 BSA-Cy5-Biotin Labeling and µ-contact Printing

Based on our experiments testing the applicability of various functionalized glass slides, streptavidin coated slides turned out to be the method of choice. This implicated the usage of BSA-Cy5 additionally conjugated with biotin. In short, BSA dissolved in borat buffer, Cy5-monoreactive dye in DMSO and biotin-cap-NHS in DMSO were mixed in various concentrations and loaded on PD-10 columns and separated into free and bound fractions. Conjugated BSA-Cy5-biotin was eluted in PBS (details in Materials and Methods sections).

The main challenge was to find an optimal ratio for the three components of the BSA-Cy5-biotin solution. First, the concentration of the BSA is fundamental for the generation of optimized BSA-grids. On the one hand too low BSA concentrations may result in an increased portion of the biotinylated ligands that also bind at the final grid position. On the other hand too high BSA concentrations may lead to unspecific blocking in the pattern regions. Second, efficient binding to the streptavidin slide can only be assured by an adequate number of conjugated biotin molecules and third, for an ideal visualization of the BSA-grid, sufficient labeling with Cy5 fluorophores is required. Our experiments testing different combinations of the three components resulted in an ideal BSA-Cy5-Biotin ratio (for details see Material and Methods), with low levels of interfering fluorescent background when visualizing the bait-prey interaction, but a sufficient amount of Cy5 fluorophores for an ideal recording of the BSA-grid (Figure 9 A1-A3). In addition, the chosen BSA concentration guaranteed efficient binding of biotinylated ligands to the functionalized glass slide. As shown in Fig. 9 an inappropriately high Cy5 concentration results in detectable fluorescence when excited at 640 nm but also at 488 nm (Figure 9 B1 and B2, respectively). Especially in case of cells that only express low levels of the fluorescent prey proteins this leads to high background levels that preclude correct contrast analysis.

Due to the protocol-change in BSA conjugation for the usage of streptavidin coated glass slides the preparation of the µ-biochips is performed as shown in Fig. 10. Noteworthy, the overall time to generate the surface is remarkably reduced compared to the procedure originally described (Schwarzenbacher, *et al.*, 2008).

4 Algorithmic Concepts for the Analysis of µ-patterning Images

4.1 Overview: Challenges in the Analysis of µ-Patterning Images

Several image preprocessing and information retrieval steps are necessary for the automated analysis of microscopy images and fluorescence contrasts in µ-patterning: The patterns in images have to be identified automatically, i.e. for each microscopy image a grid has to be found that determines the position and the size of the patterns, and for each pattern the fluorescence contrast has to be calculated with respect to the intensity background. In this section the algorithmic concepts used for solving these challenges are described: A correlation based algorithm is used for estimating the optimal downsampling rate (Section 4.2), images are transformed from grayscale to binary representation (Section 4.3), a self-adaptive evolutionary algorithm is used for identifying grids in images (Section 4.4), and finally the fluorescence contrast is calculated as described in Section 4.5.

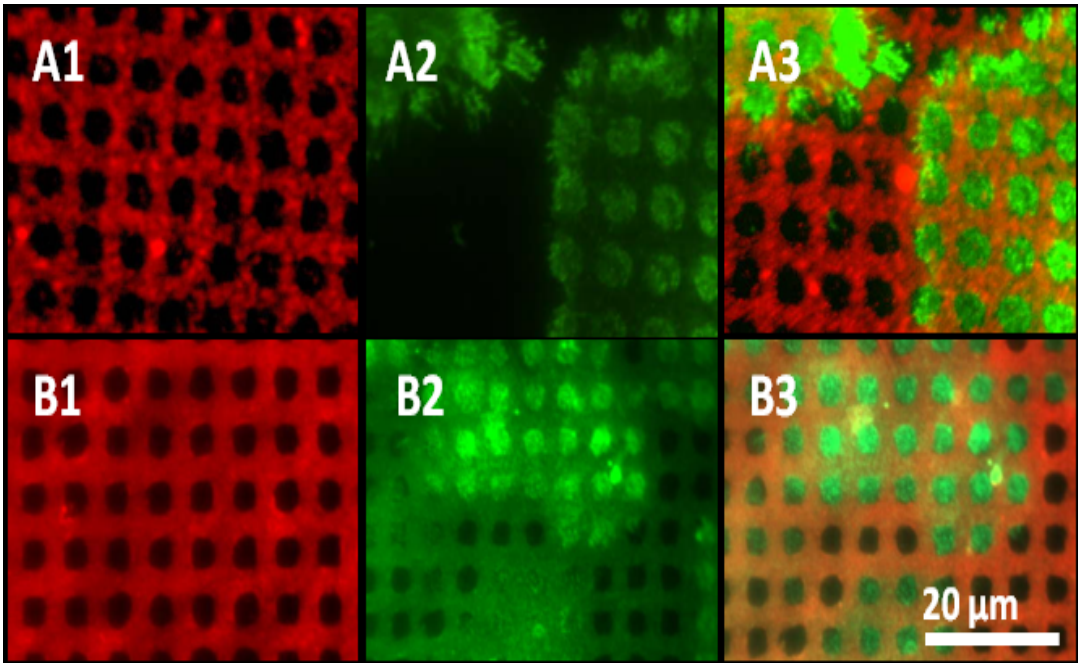

Figure 9: Influence of BSA:Cy5:Biotin ratio on BSA-Cy5 printing, ligand assembly and fluorescent background levels. T24 cells expressing GPI-GFP were grown on anti-GFP antibody functionalized Xenoprobe™ streptavidin slides. **Upper row:** ideal BSA-Cy5-Biotin ratio results in optimal BSA grid excited at 640 nm (A1) and no interfering fluorescent background at 488 nm (A2). **Bottom row:** Excessive Cy5 concentration leads to high fluorescence BSA grids (B1), but also interfering Cy5 excitation at 488 nm (B2).

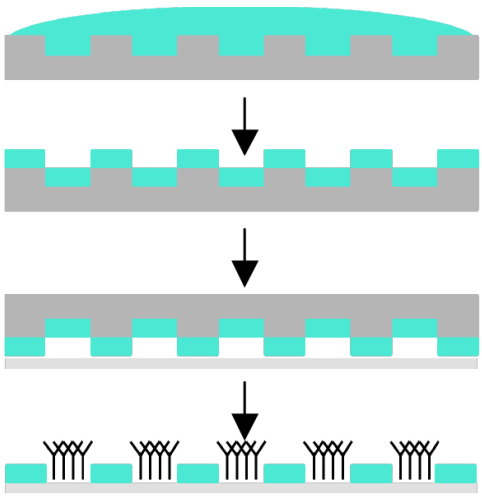

Figure 10: Principle of the µ-contact printing procedure. BSA-Cy5-Biotin-micropatterns are printed on streptavidin coated glass coverslips using a microstructured PDMS-stamp. Interspaces are directly filled with biotinylated ligands against the bait protein.

4.2 Correlation Based Optimal Downsampling

In order to decrease the runtime consumption of further image analysis steps (including the identification of grid structures), the analyzed Cy5 channel images are downsampled (Lin & Dong, 2006) using a correlation threshold θ: Starting with downsampling rate (*dsr*) 2, the *dsr* is constantly increased until the correlation (Rodgers, 1988) of the downsampled image and the original image becomes less than θ. In the following we assume that all images are given as intensities matrices, when plotted they are displayed as grayscale figures. In the simplest case, downsampling an original image *img* by factor *dsr* is defined by averaging over areas of size (*dsr* x *dsr*) for each point *p*(*x,y*). Before the correlation of this downsampled image can be compared to the original, the shrunk image has to be upscaled to the original size; in the simplest case, the copy of an image upscaled by some given factor is created by calculating the corresponding location in the original image and interpolation.

The correlation of two images img_1 and img_2 is calculated as the ratio of their mean squared deviance and the first image's intensities' variance:

$$msg(img_1, img_2) = \frac{\sum_{(x,y)\in img_1} \left((img_1)_{x,y} - (img_2)_{x,y}\right)^2}{\left|\{p : p \in img_1\}\right|}, \mathrm{var}(img) = \frac{\sum_{(x,y)\in img} \left(img_{x,y} - \overline{img}\right)^2}{\left|\{p : p \in img_1\}\right|}, \quad (1)$$

$$corr(img_1, img_2) = \frac{msd(img_1, img_2)}{\mathrm{var}(img_1)}, \quad (2)$$

where $\overline{img}$ is the average intensity of the image *img*.

Figure 11 exemplarily shows the fluorescence readout of the BSA-Cy5 grid (a) and two downscaled copies (by factors 2 and 8) with correlation 0.943 and 0.509 with the original image, respectively (b and c).

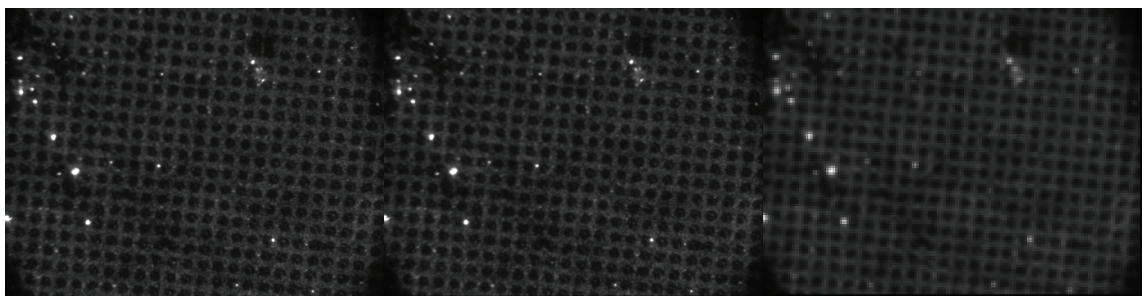

Figure 11: left: original image, **middle:** image downscaled by factor 2 and upscaled to original size (correlation 0.943 with the original), **right:** image downscaled by factor 8 and upscaled to original size (correlation 0.509 with the original).

4.3 Conversion from Grayscale to Binary Images

In order to correctly detect the BSA-Cy5 grid, pixels above a pre-defined greyscale intensity level are transformed to white representing grid pixels, others to black ones. This leads to binary images as the one exemplarily shown in Figure 12.

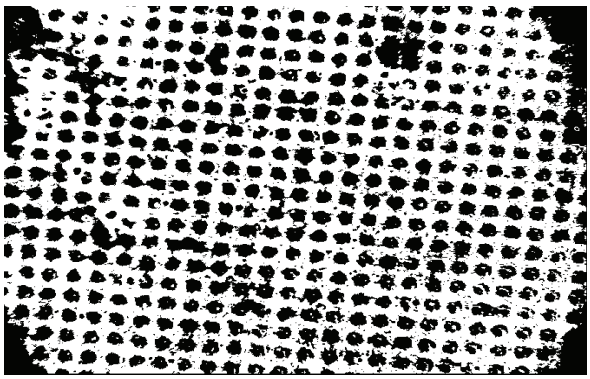

Figure 12: Binary representation of a Cy5 channel image

4.4 An Evolutionary Computation Approach for Identification of Grids in µ-Patterning Images

In this section we summarize an approach presented in (Borgmann, 2012) for identifying grid structures in images using evolution strategies: First, an initial grid is identified, which is repeatedly evaluated and mutated for creating new candidates; the best ones are promoted to the next generation.

4.4.1 Evolution Strategies

Evolution strategies (ES) are beside genetic algorithms the major representative of evolutionary computation (Rechenberg, 1973). The optimization process based on ES is executed by applying operators in a loop, i.e., main operations are applied on the solution candidates repeatedly until a given termination criterion is met. Similar to GAs, an ES works with a population of individuals; each individual is characterized by its parameter vector which is used to calculate the individual's fitness value using some predefined fitness function. In each generation of the algorithm's execution the old population is replaced by a new one. In each generation of an ES algorithm, a set of children is produced by individuals of the current population; the size of the population is denoted by μ and the number of children by λ. By selection, the best children are chosen and become the parents of the next generation. Typically, parent selection in ES is performed uniformly randomly, while survival in ES simply saves the μ best individuals.

4.4.2 Solution Candidates Representing Grids

A solution candidate is represented as a composition of four parameters and its quality measure. As shown in Figure 13, the four parameters are: the deflection of the grid (the inclination of the grid referring to the image orientation), the width of the grid (the distance between two gridlines), the horizontal offset of a reference vertical grid line, and the vertical offset of a reference horizontal grid line.

4.4.3 Identification of Initial Solution Candidates for the Optimization Process

In order to start the identification of grid structures we determine initial solution candidates which are calculated from the binary image. The first step is to define three gridlines (two vertical and one horizontal) in order to be able to complete the grid definition. A gridline itself is composed of an offset-value, which determines the position within the image, and its deflection. A gridline can be evaluated by calculating the percentage of white pixel-values compared to the binary image. Further details on the construction of initial solution candidates can be found in (Borgmann, 2012).

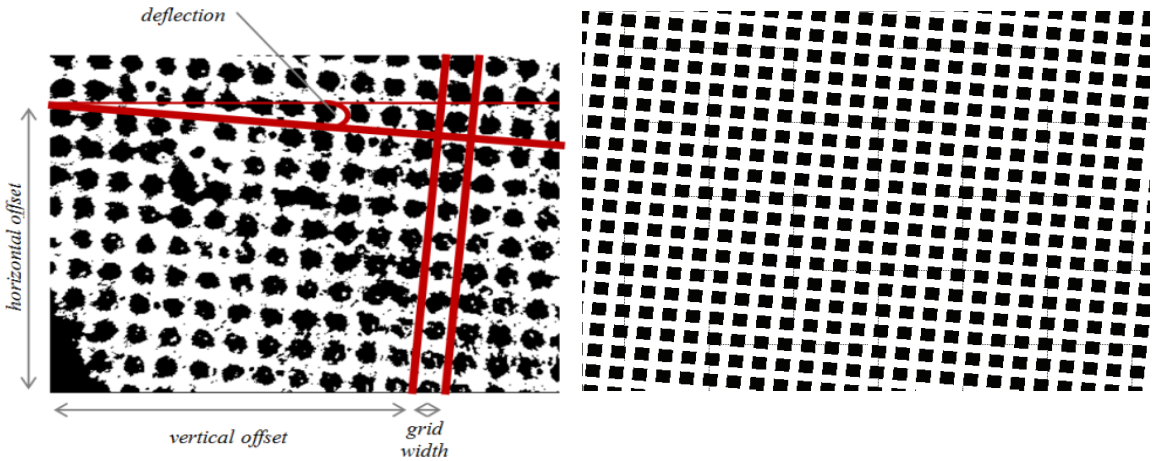

Figure 13: left: parameters of a grid candidate, **right:** exemplary expected grid. Reproduced from (Borgmann, 2012).

4.4.4 Evaluation of Grid Solution Candidates

In order to obtain a robust and reproducible comparison between various grid solution candidates and evaluation functions has been defined; this evaluation function calculates the quality of a solution candidate comparing the binary image, retrieved from the input grid image, with the solution candidate itself. As a solution candidate is only represented by four parameters, it is clearly necessary to expand the solution candidate of the size of the initial image and thus retrieve the whole grid defined by this parameter combination.

This "clamping" process is done by calculating all gridlines appearing in the initial image and furthermore a number of additional lines on the left and the right side of the original line. These additional lines are calculated to be aware of inaccuracies in the original grid picture and therefore to avoid faulty calculations of intensity and contrast values in later analysis steps.

The result of a fully clamped expected grid can be seen in Fig. 13. The result is a binary image with white-coloured grid lines and black-coloured patterns. The actual quality of a solution candidate (*grid*) is computed by the comparison of each pixel of the expected grid image (*expected (grid)*) with the corresponding pixel of the binary representation of the original image (*binary*). The number of positive comparisons is summed up over all pixels *p* and divided by the total number of pixels *N*. The retrieved value is within the range [0, 1].

$$N(binary) = \left|\{p \mid p \in binary\}\right|; P(grid, binary) = \left|\{expected(grid)[p] = binary[p]\}\right| \tag{3}$$

$$quality(grid, binary) = \frac{\left|P(grid, binary)\right|}{\left|N(binary)\right|} \tag{4}$$

4.4.5 Rotation of Images Using Identified Grids

For enabling a more user-friendly display of the analyzed µ-pattering images, we rotate the image in the opposite direction of the deflection of the identified grid. The rotation angle α is calculated as:

$$\alpha = -\tan(g.deflection). \tag{5}$$

This rotation is executed using the well-known rotation matrix (Goldstein, 2002):

$$r = \begin{bmatrix} \cos\alpha & -\sin\alpha \\ \sin\alpha & \cos\alpha \end{bmatrix} \tag{6}$$

4.4.6 Examples

In Figure 14 we exemplarily show the identification of a grid on a µ-patterning image: The initially constructed image is shown as well as the solutions found by an ES (µ = 5, λ = 10, downsampling tolerance 0.9) after 10, 20, and 40 iterations with qualities 0.62, 0.71, and 0.72, respectively (from left to right). While the initially constructed grid cannot be considered appropriate, the algorithm automatically optimizes the grid parameters and, eventually after 40 iterations, produces a grid that correctly fits the µ-patterned structure.

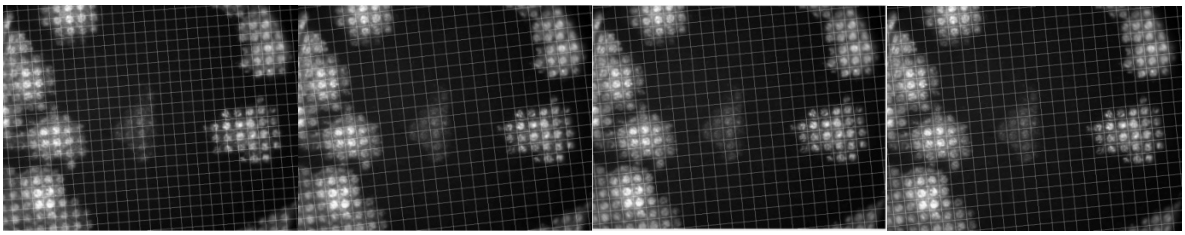

Figure 14: Grid improvement during the ES process (m = 5, l = 10, downsampling tolerance 0.9); initial solution (quality: 0.55), after 10 iterations (quality: 0.62), after 20 iterations (quality: 0.71), after 40 iterations (final grid quality: 0.72) from left to right.

Further examples and performance comparisons of different ES configurations can be found in (Borgmann, 2012). For the image shown in Figure 11 the deflection of the identified grid is 0.1, so it has to be rotated by -10.03°; Figure 15 shows the image of Figure 11 rotated by 10.03° counter-clockwise.

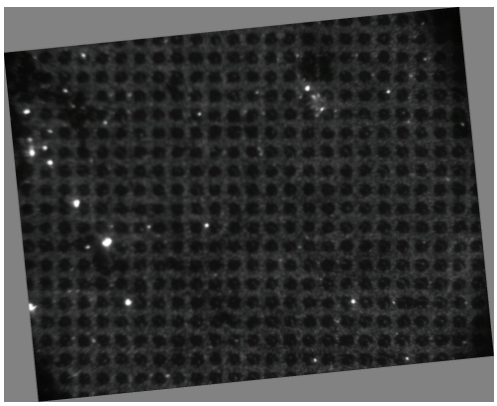

Figure 15: Image shown in Figure 11 rotated by ~10° counter-clockwise

4.5 Fluorescence Contrast Analysis

Based on the correct identification of the grid position with respect to fluorescent patterns, the fluorescence contrast can be calculated for each pattern in the image as:

$$C = \frac{F^{+} - F^{-}}{F^{+} - F_{BG}} \tag{7}$$

where F^{+} denotes the intensity of the inner pixels of the µ-pattern, F^{-} the intensity of the background (i.e. the intensity of the surrounding pixels of µp), and F_{BG} the intensity of the global background as originally described in (Schwarzenbacher, *et al.*, 2008).

A relevant factor in this context is the size of the F^{+} region, i.e., the region of the grid cell in which the prey redistribution becomes visible. The definition of this F^{+} region is a crucible factor for the success of contrast evaluation, the size of the F^{+} region has to be adjusted to the size of the PDMS based µ-patterns. E.g., in Figure 16 we see an enlarged view of a µ-pattern for which the F^{+} region is defined and depicted by yellow circles. The F^{+} region diameter is set to 30%, 80%, and 60% of the grid cells' width, respectively. As we see, 60% is in this case the ideal choice for the calculation of the contrast.

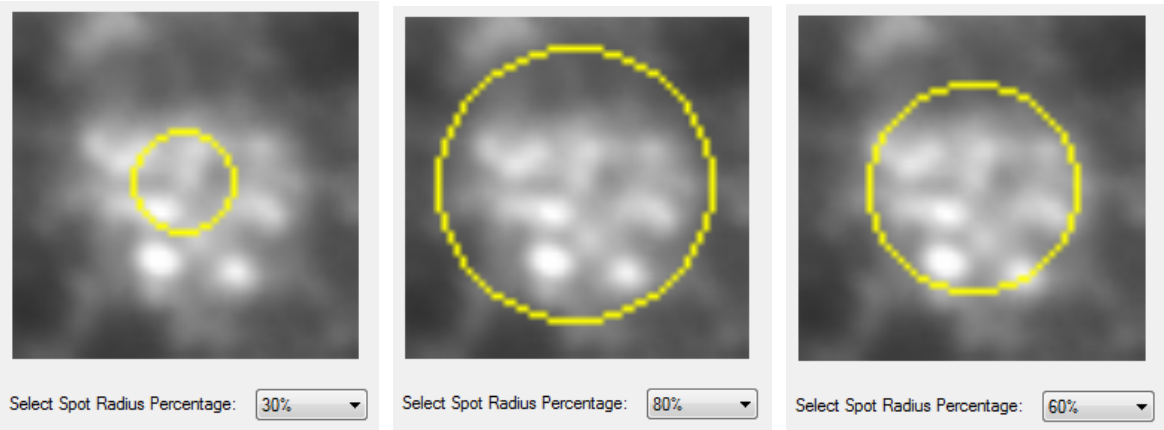

Figure 16: Definition of circular F^{+} regions with varying spot radius. The F^{+} region diameter is set to 30%, 80%, and 60% of the grid cells' width, respectively.

5 New Applications of the µ-patterning Approach

5.1 Targeting Bait Proteins with Limited Epitope Accessibility

We have recently realized that an epitope of the bait protein may not be accessible for a µ-biochip bound antibody in some cases. Possible reasons for that can be steric hindrance, heavy protein modifications (e.g. glycosylation) or the shielding of the binding site by genetically fused tags, especially large fluorescent proteins. In some cases we found out that variations in the length of the bait ligand can help to better access the epitope of the bait protein. As an example we present here the redistribution of the glucose transporter 4 (Glut4) on antibody coated µ-biochips. Upon insulin stimulation the Glut4 transporter is translocated to the plasma membrane and lowers the blood glucose level by transporting glucose into the

cells (Watson, Kanzaki, & Pessin, 2004; Watson *et al.*, 2004). Monitoring this translocation has become an important tool in the search for insulin signaling interfering drugs. Therefore, rather indirect methods such as western blot analysis of plasma membrane fractions or photoaffinity labeling, but also qualitative measurements based on immunofluorescence are used for the investigation on insulin- or insulin-mimetic drug-stimulated GLUT4 translocation (Baus *et al.*, 2010; Boguslavsky *et al.*, 2012; Kozka, Clark, & Holman, 1991). An important improvement has been the visualization of dual-tagged Glut4 transporters by 2-color confocal microscopy. In order to benefit from the advantages of TIRF-microscopy for an easier and more reliable quantification, we analyzed the translocation of Glut4 in live cells using the µ-patterning approach. For that purpose we stably expressed a dual-tagged Glut4 construct with an intracellular GFP and a myc-tag in the loop connecting the first two transmembrane domains of the protein (Williams & Pessin, 2008) and grew the cells on anti-myc antibody coated µ-biochips. As indicated in Figure 17A there was only minor redistribution of the bait protein. We therefore changed our strategy and grew the same cells on µ-biochips coated with a primary anti-mouse IgG bound to the glass-surface and an anti-myc antibody captured by the primary antibody. Indeed, as shown in Fig. 17 B, we detected a strong redistribution of Glut4 in such experiments. We conclude that the usage of larger or more flexible ligands enables the binding of bait epitopes that are difficult to access by single antibodies.

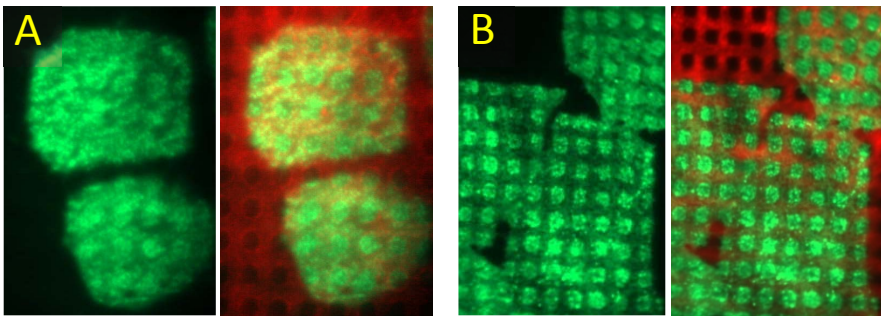

Figure 17: µ-patterning experiments of glucose transporter 4 (Glut4). HeLa cells stably expressing Glut4-myc-GFP were grown on anti-myc antibody (A – low contrast) or anti-mouse IgG and anti-myc antibody (B – high contrast) coated µ-biochips, respectively.

5.2 Interaction Studies of Receptor Tyrosine Kinases

A group of membrane proteins of special interest are receptor tyrosine kinases (RTKs). These high-affinity cell surface receptors for many polypeptide growth factors, cytokines and hormones have been shown to be key regulators of numerous cellular processes (Robinson, Wu, & Lin, 2000). Furthermore they have a critical role in the development and progression of many types of cancer (Zwick, Bange, & Ullrich, 2001). Thus these receptors are common targets for drug screening. So far approximately 20 different human RTK classes encoding nearly 60 RTK proteins have been identified, among them the epidermal growth factor receptor (EGFR or ErbB) family (RTK class I) (Robinson, *et al.*, 2000).

The EGFR plays a major role in cellular signaling: insufficient signaling may lead to the development of neurodegenerative diseases (Bublil & Yarden, 2007), while excessive EGFR signaling is associated with the development of a wide variety of tumors. Highly elevated EGFR signaling seems to be a critical factor in the development and malignancy of these tumors (Cho & Leahy, 2002).

We are currently investigating the interaction properties of the EGFR using the µ-patterning approach. Therefore we are interested in the interaction of this receptor with intracellular binding partners. One protein that has been reported to interact with the EGFR is the growth factor receptor-bound protein 2 (Grb2). It is a widely expressed adaptor protein with one SH2 and two SH3 domains to bind tyrosine phosphorylated sequences and proline-rich regions, respectively (Lowenstein *et al.*, 1992; Matuoka, Shibata, Yamakawa, & Takenawa, 1992). Grb2 is best known for its ability to link the EGFR to the activation of Ras and further downstream kinases ERK1 and 2 (Okutani *et al.*, 1994).

Quantification of EGFR signaling with downstream molecules (e.g. Grb2) is usually based on immunoprecipitation (IP) experiments of the EGFR and co-precipitation of the corresponding intracellular interaction partner (Kholodenko, Demin, Moehren, & Hoek, 1999; Stang *et al.*, 2004; Yamazaki *et al.*, 2002). Co-IP implicates several disadvantages including an unavailable option for monitoring receptor signaling *in-vivo*. In the last few years live cell approaches based on fluorescent microscopy and gene reporter assays covering this necessity were developed (W. Li *et al.*, 2008; Morimatsu *et al.*, 2007). We believe that the µ-patterning technique might serve as a valuable tool for the analysis of the EGFR and other receptor tyrosine kinases with intracellular binding partners.

As already described it is possible to detect and quantify the effects of externally added drugs (e.g. a chelator) on the interaction of bait and prey in live cells using the µ-patterning approach (Schwarzenbacher, *et al.*, 2008). Due to the fact that both EGFR and IR are important targets for drug screening, it is our aim to visualize the interaction of EGFR or IR with intracellular binding partners (e.g. Grb2) by µ-patterning experiments, and quantify changes in the interaction strength after addition of drugs.

We focus on secondary plant metabolites, which are known to reduce the EGFR tyrosine kinase activity (Schlupper, Giesa, & Gebhardt, 2006), inhibit neoplastic transformation of cells (Dong, 2000; Mechikova *et al.*, 2010) or enhance the toxicity of EGF-targeted toxins (Bachran *et al.*, 2010). However, molecular data proofing the direct influence of such drugs on the interaction of signaling proteins in live cells are missing.

To address this question we visualized the interaction of the EGFR with Grb2. Therefore we stably expressed Grb2-YFP in HeLa cells and seeded them on anti-EGFR antibody coated µ-biochips. As shown in Figure 18A we found a prominent redistribution of Grb2 to endogenously expressed EGFR enriched regions indicating interaction of these two proteins. We analyzed the contrast of ~900 patterns from 70 cells and calculated a remarkable mean contrast of 0.265 (Figure 18B).

6 Conclusions

The µ-patterning assay has become a promising and valuable tool to analyze and quantify protein-protein-interactions in a live cell context. Making the application faster and more reliable was an important step in order to address new biological questions within limited time. Together with the development of user-friendly customized software, the applicability of the assay also for other researchers working in a wide variety of scientific fields has been remarkably increased.

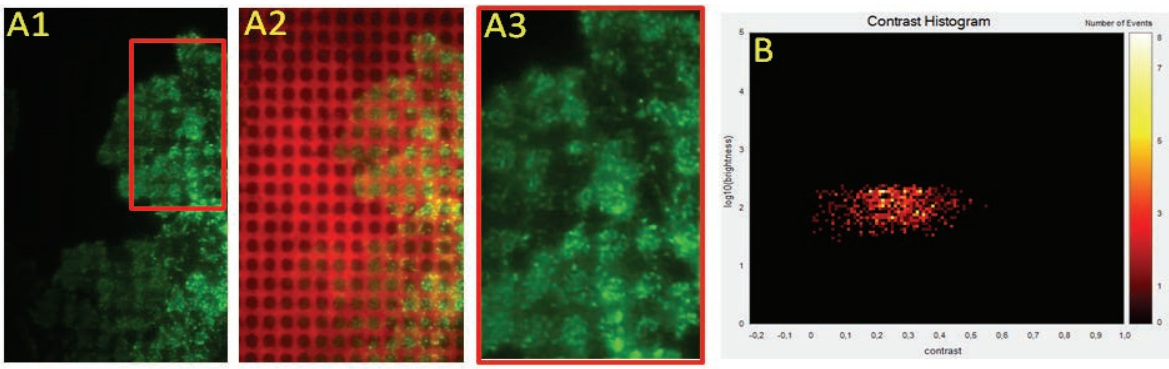

Figure 18: Interaction of Grb2 with the EGF receptor. (A) HeLa cells stably expressing Grb2-YFP were grown on anti-EGFR antibody coated µ-biochips (A1-2). Patterns indicate interaction of these two proteins. An enlarged view is marked by the red square (A3). (B). Analysis of 70 cells is shown in a color density plot for the fluorescence brightness F^+ and mean contrast (C).

7 Materials and Methods

7.1 DNA constructs and reagents

The pcDNA3-GLUT4-myc-GFP was kindly provided by J.E. Pessin (Albert Einstein College of Medicine, New York) and the pcDNA3-Grb2-YFP was a kind gift from L.E. Samelson, (NIH, Bethesda). The monoclonal antibodies against the EGFR were purchased from Antibodies online, Herford, Germany, the anti-mouse IgG was from Sigma-Aldrich (Schnellendorf, Germany) and the anti-myc antibody was purchased from Santa Cruz (Heidelberg, Germany).

7.2 Cell culture

Media, fetal bovine serum (FBS), antibiotics and Geneticin (G418 sulfate) were purchased from PAA Laboratories GmbH, Pasching, Austria. Culture plates were from Greiner Bio One International, Austria. Human HeLa cells were from American Type Culture Collection. An electroporation unit (Nucleofector) and electroporation cuvettes were from Lonza, Basel, Switzerland.

HeLa cells were cultured in RPMI medium supplemented with 10 % FBS and penicillin/streptomycin and grown at 37 °C in a humidified incubator (≥ 95 %) with 5 % CO_2. The day before transfection the cells were subcultured and transfected the day after at 50-70 % confluence with 1-5 µg DNA using the Nucleofector device. For transfection RPMI without FBS and P/S was used. Cells were plated into 60-mm culture dishes and grown for 48 h. The medium was removed and replaced with fresh medium supplemented with 400 µg/ml G418. Medium was changed every 3 days and 15-20 days later individual neomycin-resistant colonies were selected for propagation and analysis.

7.3 BSA-Cy5-Biotin preparation and µ-contact printing

In order to successfully use streptavidin coated glass slides it was necessary to alter the µ-contact printing procedure including new labeling of BSA-Cy5-Biotin. In short, BSA (1 mg, 30 nmol) was dissolved in 0.5 ml of borat buffer (25 mM, pH 8.6). In addition, a complete Cy5-Monoreactive Dye (GE Healthcare

Life Sciences, PA25001) was dissolved in 0.5 ml DMSO. 2 µl of the Cy5-DMSO solution were then added to the BSA solution, mixed and incubated for 30 min with occasional vortexing. After incubation 5 µl of 12 mM Biotin-cap-NHS (Sigma-Aldrich, B2643) in DMSO (5.45 mg/ml, 120 nmol) were added while vortexing. The mixture was incubated for 30 min in the dark with occasional vortexing. In the meanwhile a PD-10 desalting column (GE Healthcare Life Sciences, 17-0851-01) was pre-equilibrated with 20 ml PBS. The BSA-Cy5-Biotin solution was then loaded onto the column and separated into free and bound fractions. Conjugated and ready-to-use BSA-Cy5-Biotin was finally eluted in 1.5 ml PBS.

This purified solution could be then used for the simplified and shortened µ-contact printing procedure on streptavidin-coated glass slides (Figure 10). First, the micropattern field of a prepared PDMS stamp (polydimethylsiloxan) is cut out. The field is then washed by flushing with ethanol (100%) and distilled water and dried with nitrogen. 20 µl BSA-Cy5-Biotin solution is then pipetted onto the micropattern field (the whole field must be covered with solution). The cutout PDMS is incubated for 15 min at room temperature in the dark. After incubation it is washed by flushing with phosphate buffered saline (PBS) and distilled water and dried with nitrogen. The prepared PDMS stamp is then placed on a streptavidin-coated coverslip (Xenoprobe^{TM} Streptavidin) and incubated for 30 min at room temperature in a petri dish in the dark. Before removal of the PDMS stamp the micropattern field is labeled on the back of the coverslip helping to place a Secure Seal Hybridization chamber (Sigma, C0975) on the microcontact-printed field. The reaction chamber is filled with 60 µl of biotinylated antibody solution (10 µg/ml in PBST; containing 0.1 % Tween 20) and incubated for 1 h at room temperature. After incubation the sample is washed with 1 ml PBST and the micropatterned surfaces are ready to use or can be stored over night at 4 °C in PBS.

7.4 Microscopy

The detection system was set up on an epi-fluorescence microscope (Olympus IX81). Diode lasers (iBeam smart, Toptica, Germany) were used for selective fluorescence excitation of GFP, YFP and Cy5 at 488 nm, 514 nm and 640 nm, respectively. Samples were illuminated in total internal reflection (TIR) configuration (Cell^{TIRF}, Olympus) using a 60 x oil immersion objective (NA = 1.49, APON 60XO TIRF, Olympus, Germany). After appropriate filtering using standard filter sets, fluorescence was imaged onto a CCD camera (Orca-R2, Hamamatsu, Japan). Readout was performed in an automatic partial range scan mode using a motorized xy-microscopy stage (Märzhäuser, Germany). The reader was equipped with an automated focus hold system (ZDC). All scans were performed in sequential performance (with short time delay) in two colors, with one scan at 488 nm (or 514 nm) for selective excitation of GFP (or YFP), the second scan at 640 nm for selective excitation of Cy5. Filters were changed automatically within the scan process. All scans were recorded at room temperature.

Acknowledgements

We thank J.E. Pessin (Albert Einstein College of Medicine, New York) and L.E. Samelson, (NIH, Bethesda) for providing DNA constructs. This work was funded by the program “Regionale Wettbewerbsfähigkeit OÖ 2007-2013” with financial means of the European fund for regional development as well as the country of Upper Austria.

References

Alberts, B., & Miake-Lye, R. (1992). Unscrambling the puzzle of biological machines: the importance of the details. Cell, 68(3), 415-420.

Alexander, R. A., Prager, G. W., Mihaly-Bison, J., Uhrin, P., Sunzenauer, S., Binder, B. R., et al. (2012). VEGF-induced endothelial cell migration requires urokinase receptor (uPAR)-dependent integrin redistribution. Cardiovasc Res, 94(1), 125-135.

Axelrod, D. (2003). Total internal reflection fluorescence microscopy in cell biology. Methods Enzymol, 361, 1-33.

Bachran, D., Schneider, S., Bachran, C., Urban, R., Weng, A., Melzig, M. F., et al. (2010). Epidermal growth factor receptor expression affects the efficacy of the combined application of saponin and a targeted toxin on human cervical carcinoma cells. Int J Cancer, 127(6), 1453-1461.

Barrios-Rodiles, M., Brown, K. R., Ozdamar, B., Bose, R., Liu, Z., Donovan, R. S., et al. (2005). High-throughput mapping of a dynamic signaling network in mammalian cells. Science, 307(5715), 1621-1625.

Baus, D., Yan, Y., Li, Z., Garyantes, T., de Hoop, M., & Tennagels, N. (2010). A robust assay measuring GLUT4 translocation in rat myoblasts overexpressing GLUT4-myc and AS160_v2. Anal Biochem, 397(2), 233-240.

Blackburn, J. M., & Shoko, A. (2011). Protein function microarrays for customised systems-oriented proteome analysis. Methods Mol Biol, 785, 305-330.

Blackburn, J. M., Shoko, A., & Beeton-Kempen, N. (2012). Miniaturized, microarray-based assays for chemical proteomic studies of protein function. Methods Mol Biol, 800, 133-162.

Boguslavsky, S., Chiu, T., Foley, K. P., Osorio-Fuentealba, C., Antonescu, C. N., Bayer, K. U., et al. (2012). Myo1c binding to submembrane actin mediates insulin-induced tethering of GLUT4 vesicles. Mol Biol Cell, 23(20), 4065-4078.

Borgmann, D. M., Weghuber, J., Schaller, S., Jacak, J., Winkler, S.M. (2012). Identification of Patterns in Microscopy Images of Biological Samples Using Evolution Strategies. Proceedings of the 24th European Modeling and Simulation Symposium.

Brameshuber, M., Schwarzenbacher, M., Kaltenbrunner, M., Hesch, C., Paster, W., Weghuber, J., Heis, B., Sonnleitner, A., Stockinger, H., Schütz, G.J. (2009). Reply to "Uncoupling diffusion and binding in FRAP experiments". Nature Methods, 6, 183-184.

Bublil, E. M., & Yarden, Y. (2007). The EGF receptor family: spearheading a merger of signaling and therapeutics. Curr Opin Cell Biol, 19(2), 124-134.

Bucci, E., Fronticelli, C., Chiancone, E., Wyman, J., Antonini, E., & Rossi-Fanelli, A. (1965). The Properties and Interactions of the Isolater Alpha and Beta Chains of Human Haemoglobin. I. Sedimentation and Electrophoretic Behaviour. J Mol Biol, 12, 183-192.

Cavalcanti-Adam, E. A., Micoulet, A., Blummel, J., Auernheimer, J., Kessler, H., & Spatz, J. P. (2006). Lateral spacing of integrin ligands influences cell spreading and focal adhesion assembly. Eur J Cell Biol, 85(3-4), 219-224.

Cho, H. S., & Leahy, D. J. (2002). Structure of the extracellular region of HER3 reveals an interdomain tether. Science, 297(5585), 1330-1333.

Cohen, G. B., Ren, R., & Baltimore, D. (1995). Modular binding domains in signal transduction proteins. Cell, 80(2), 237-248.

Deane, C. M., Salwinski, L., Xenarios, I., & Eisenberg, D. (2002). Protein interactions: two methods for assessment of the reliability of high throughput observations. Mol Cell Proteomics, 1(5), 349-356.

Digman, M. A., Wiseman, P. W., Choi, C., Horwitz, A. R., & Gratton, E. (2009). Stoichiometry of molecular complexes at adhesions in living cells. Proc Natl Acad Sci U S A, 106(7), 2170-2175.

Dong, Z. (2000). Effects of food factors on signal transduction pathways. Biofactors, 12(1-4), 17-28.

Dorsch, S., Klotz, K. N., Engelhardt, S., Lohse, M. J., & Bunemann, M. (2009). Analysis of receptor oligomerization by FRAP microscopy. Nat Methods, 6(3), 225-230.

Ewing, R. M., Chu, P., Elisma, F., Li, H., Taylor, P., Climie, S., et al. (2007). Large-scale mapping of human protein-protein interactions by mass spectrometry. Mol Syst Biol, 3, 89.

Fields, S., & Song, O. (1989). A novel genetic system to detect protein-protein interactions. Nature, 340(6230), 245-246.

Förster, T. (1948). Intermolecular energy migration and fluorescence. Ann Phys, 6, 55-75.

Gavin, A. C., Bosche, M., Krause, R., Grandi, P., Marzioch, M., Bauer, A., et al. (2002). Functional organization of the yeast proteome by systematic analysis of protein complexes. Nature, 415(6868), 141-147.

Goldstein, H., Poole, C.P., Safko, J.L. (2002). Classical Mechanics: Addison Wesley.

Golemis, E. (Ed.). (2005). Protein-protein interactions: A molecular cloning manual: Cold Spring Harbor, NY: Cold Spring Harbor Laboratory Press.

Haslam, R. J., Koide, H. B., & Hemmings, B. A. (1993). Pleckstrin domain homology. Nature, 363(6427), 309-310.

Hino, N., Okazaki, Y., Kobayashi, T., Hayashi, A., Sakamoto, K., & Yokoyama, S. (2005). Protein photo-cross-linking in mammalian cells by site-specific incorporation of a photoreactive amino acid. Nat Methods, 2(3), 201-206.

Hu, C. D., Chinenov, Y., & Kerppola, T. K. (2002). Visualization of interactions among bZIP and Rel family proteins in living cells using bimolecular fluorescence complementation. Mol Cell, 9(4), 789-798.

Hurt, J. A., Thibodeau, S. A., Hirsh, A. S., Pabo, C. O., & Joung, J. K. (2003). Highly specific zinc finger proteins obtained by directed domain shuffling and cell-based selection. Proc Natl Acad Sci U S A, 100(21), 12271-12276.

James, P. (1997). Protein identification in the post-genome era: the rapid rise of proteomics. Q Rev Biophys, 30(4), 279-331.

Jares-Erijman, E. A., & Jovin, T. M. (2003). FRET imaging. Nat Biotechnol, 21(11), 1387-1395.

Junttila, M. R., Saarinen, S., Schmidt, T., Kast, J., & Westermarck, J. (2005). Single-step Strep-tag purification for the isolation and identification of protein complexes from mammalian cells. Proteomics, 5(5), 1199-1203.

Kane, R. S., Takayama, S., Ostuni, E., Ingber, D. E., & Whitesides, G. M. (1999). Patterning proteins and cells using soft lithography. Biomaterials, 20(23-24), 2363-2376.

Kerppola, T. K. (2006). Visualization of molecular interactions by fluorescence complementation. Nat Rev Mol Cell Biol, 7(6), 449-456.

Kholodenko, B. N., Demin, O. V., Moehren, G., & Hoek, J. B. (1999). Quantification of short term signaling by the epidermal growth factor receptor. J Biol Chem, 274(42), 30169-30181.

Kolisek, M., Zsurka, G., Samaj, J., Weghuber, J., Schweyen, R. J., & Schweigel, M. (2003). Mrs2p is an essential component of the major electrophoretic Mg2+ influx system in mitochondria. EMBO J, 22(6), 1235-1244.

Koolwijk, P., Sidenius, N., Peters, E., Sier, C. F., Hanemaaijer, R., Blasi, F., et al. (2001). Proteolysis of the urokinase-type plasminogen activator receptor by metalloproteinase-12: implication for angiogenesis in fibrin matrices. Blood, 97(10), 3123-3131.

Kozka, I. J., Clark, A. E., & Holman, G. D. (1991). Chronic treatment with insulin selectively down-regulates cell-surface GLUT4 glucose transporters in 3T3-L1 adipocytes. J Biol Chem, 266(18), 11726-11731.

Krogan, N. J., Cagney, G., Yu, H., Zhong, G., Guo, X., Ignatchenko, A., et al. (2006). Global landscape of protein complexes in the yeast Saccharomyces cerevisiae. Nature, 440(7084), 637-643.

Li, Q. J., Dinner, A. R., Qi, S., Irvine, D. J., Huppa, J. B., Davis, M. M., et al. (2004). CD4 enhances T cell sensitivity to antigen by coordinating Lck accumulation at the immunological synapse. Nat Immunol, 5(8), 791-799.

Li, W., Li, F., Huang, Q., Frederick, B., Bao, S., & Li, C. Y. (2008). Noninvasive imaging and quantification of epidermal growth factor receptor kinase activation in vivo. Cancer Res, 68(13), 4990-4997.

Lin, W., & Dong, L. (2006). Adaptive downsampling to improve image compression at low bit rates. IEEE Trans Image Process, 15(9), 2513-2521.

Lowenstein, E. J., Daly, R. J., Batzer, A. G., Li, W., Margolis, B., Lammers, R., et al. (1992). The SH2 and SH3 domain-containing protein GRB2 links receptor tyrosine kinases to ras signaling. Cell, 70(3), 431-442.

Lunin, V. V., Dobrovetsky, E., Khutoreskaya, G., Zhang, R., Joachimiak, A., Doyle, D. A., et al. (2006). Crystal structure of the CorA Mg2+ transporter. Nature, 440(7085), 833-837.

Matuoka, K., Shibata, M., Yamakawa, A., & Takenawa, T. (1992). Cloning of ASH, a ubiquitous protein composed of one Src homology region (SH) 2 and two SH3 domains, from human and rat cDNA libraries. Proc Natl Acad Sci U S A, 89(19), 9015-9019.

Mayer, B. J. (2001). SH3 domains: complexity in moderation. J Cell Sci, 114(Pt 7), 1253-1263.

Mechikova, G. Y., Kuzmich, A. S., Ponomarenko, L. P., Kalinovsky, A. I., Stepanova, T. A., Fedorov, S. N., et al. (2010). Cancer-preventive activities of secondary metabolites from leaves of the bilberry Vaccinium smallii A. Gray. Phytother Res, 24(11), 1730-1732.

Morimatsu, M., Takagi, H., Ota, K. G., Iwamoto, R., Yanagida, T., & Sako, Y. (2007). Multiple-state reactions between the epidermal growth factor receptor and Grb2 as observed by using single-molecule analysis. Proc Natl Acad Sci U S A, 104(46), 18013-18018.

Mossman, K. D., Campi, G., Groves, J. T., & Dustin, M. L. (2005). Altered TCR signaling from geometrically repatterned immunological synapses. Science, 310(5751), 1191-1193.

Okutani, T., Okabayashi, Y., Kido, Y., Sugimoto, Y., Sakaguchi, K., Matuoka, K., et al. (1994). Grb2/Ash binds directly to tyrosines 1068 and 1086 and indirectly to tyrosine 1148 of activated human epidermal growth factor receptors in intact cells. J Biol Chem, 269(49), 31310-31314.

Pawson, T. (1995). Protein modules and signalling networks. Nature, 373(6515), 573-580.

Pawson, T., Gish, G. D., & Nash, P. (2001). SH2 domains, interaction modules and cellular wiring. Trends Cell Biol, 11(12), 504-511.

Pawson, T., & Nash, P. (2003). Assembly of cell regulatory systems through protein interaction domains. Science, 300(5618), 445-452.

Pawson, T., & Scott, J. D. (1997). Signaling through scaffold, anchoring, and adaptor proteins. Science, 278(5346), 2075-2080.

Pfleger, K. D., & Eidne, K. A. (2006). Illuminating insights into protein-protein interactions using bioluminescence resonance energy transfer (BRET). Nat Methods, 3(3), 165-174.

Phizicky, E. M., & Fields, S. (1995). Protein-protein interactions: methods for detection and analysis. Microbiol Rev, 59(1), 94-123.

Pike, L. J. (2006). Rafts defined: a report on the Keystone Symposium on Lipid Rafts and Cell Function. J Lipid Res, 47(7), 1597-1598.

Pollok, B. A., & Heim, R. (1999). Using GFP in FRET-based applications. Trends Cell Biol, 9(2), 57-60.

Ponting, C. P., & Russell, R. R. (2002). The natural history of protein domains. Annu Rev Biophys Biomol Struct, 31, 45-71.

Prager, G. W., Mihaly, J., Brunner, P. M., Koshelnick, Y., Hoyer-Hansen, G., & Binder, B. R. (2009). Urokinase mediates endothelial cell survival via induction of the X-linked inhibitor of apoptosis protein. Blood, 113(6), 1383-1390.

Puig, O., Caspary, F., Rigaut, G., Rutz, B., Bouveret, E., Bragado-Nilsson, E., et al. (2001). The tandem affinity purification (TAP) method: a general procedure of protein complex purification. Methods, 24(3), 218-229.

Rebecchi, M. J., & Scarlata, S. (1998). Pleckstrin homology domains: a common fold with diverse functions. Annu Rev Biophys Biomol Struct, 27, 503-528.

Rechenberg, I. (1973). Evolutionsstrategie: Friedrich Frommann Verlag.

Regoes, A., & Hehl, A. B. (2005). SNAP-tag mediated live cell labeling as an alternative to GFP in anaerobic organisms. Biotechniques, 39(6), 809-810, 812.

Robinson, D. R., Wu, Y. M., & Lin, S. F. (2000). The protein tyrosine kinase family of the human genome. Oncogene, 19(49), 5548-5557.

Rodgers, J. L., Nicewander, W.A. (1988). Thirteen ways to look at the correlation coefficient. The American Statistician 42, 59-66.

Ruprecht, V., Weghuber, J., Wieser, S., Schütz, G.J. (2010). Measuring Colocalization by Dual Color Single Molecule Imaging: Thresholds, Error Rates, and Sensitivity. Advances in Planar Lipid Bilayers and Liposomes, 12, 21-40.

Sadowski, I., Stone, J. C., & Pawson, T. (1986). A noncatalytic domain conserved among cytoplasmic protein-tyrosine kinases modifies the kinase function and transforming activity of Fujinami sarcoma virus P130gag-fps. Mol Cell Biol, 6(12), 4396-4408.

Schlupper, D., Giesa, S., & Gebhardt, R. (2006). Influence of biotransformation of luteolin, luteolin 7-O-glucoside, 3',4'-dihydroxyflavone and apigenin by cultured rat hepatocytes on antioxidative capacity and inhibition of EGF receptor tyrosine kinase activity. Planta Med, 72(7), 596-603.

Schmidt, T. G., & Skerra, A. (2007). The Strep-tag system for one-step purification and high-affinity detection or capturing of proteins. Nat Protoc, 2(6), 1528-1535.

Schwarzenbacher, M., Kaltenbrunner, M., Brameshuber, M., Hesch, C., Paster, W., Weghuber, J., et al. (2008). Micropatterning for quantitative analysis of protein-protein interactions in living cells. Nat Methods, 5(12), 1053-1060.

Schwille, P., Meyer-Almes, F. J., & Rigler, R. (1997). Dual-color fluorescence cross-correlation spectroscopy for multicomponent diffusional analysis in solution. Biophys J, 72(4), 1878-1886.

Shaner, N. C., Campbell, R. E., Steinbach, P. A., Giepmans, B. N., Palmer, A. E., & Tsien, R. Y. (2004). Improved monomeric red, orange and yellow fluorescent proteins derived from Discosoma sp. red fluorescent protein. Nat Biotechnol, 22(12), 1567-1572.

Sharon, M., & Robinson, C. V. (2007). The role of mass spectrometry in structure elucidation of dynamic protein complexes. Annu Rev Biochem, 76, 167-193.

Soderberg, O., Gullberg, M., Jarvius, M., Ridderstrale, K., Leuchowius, K. J., Jarvius, J., et al. (2006). Direct observation of individual endogenous protein complexes in situ by proximity ligation. Nat Methods, 3(12), 995-1000.

Stagljar, I., Korostensky, C., Johnsson, N., & te Heesen, S. (1998). A genetic system based on split-ubiquitin for the analysis of interactions between membrane proteins in vivo. Proc Natl Acad Sci U S A, 95(9), 5187-5192.

Stang, E., Blystad, F. D., Kazazic, M., Bertelsen, V., Brodahl, T., Raiborg, C., et al. (2004). Cbl-dependent ubiquitination is required for progression of EGF receptors into clathrin-coated pits. Mol Biol Cell, 15(8), 3591-3604.

Stelzl, U., Worm, U., Lalowski, M., Haenig, C., Brembeck, F. H., Goehler, H., et al. (2005). A human protein-protein interaction network: a resource for annotating the proteome. Cell, 122(6), 957-968.

Stryer, L., & Haugland, R. P. (1967). Energy transfer: a spectroscopic ruler. Proc Natl Acad Sci U S A, 58(2), 719-726.

Suchanek, M., Radzikowska, A., & Thiele, C. (2005). Photo-leucine and photo-methionine allow identification of protein-protein interactions in living cells. Nat Methods, 2(4), 261-267.

Sunzenauer, S., Zojer, V., Brameshuber, M., Trols, A., Weghuber, J., Stockinger, H., et al. (2012). Determination of binding curves via protein micropatterning in vitro and in living cells. Cytometry A.

Swanson, K. A., Kang, R. S., Stamenova, S. D., Hicke, L., & Radhakrishnan, I. (2003). Solution structure of Vps27 UIM-ubiquitin complex important for endosomal sorting and receptor downregulation. EMBO J, 22(18), 4597-4606.

Synowsky, S. A., van den Heuvel, R. H., Mohammed, S., Pijnappel, P. W., & Heck, A. J. (2006). Probing genuine strong interactions and post-translational modifications in the heterogeneous yeast exosome protein complex. Mol Cell Proteomics, 5(9), 1581-1592.

Tagwerker, C., Flick, K., Cui, M., Guerrero, C., Dou, Y., Auer, B., et al. (2006). A tandem affinity tag for two-step purification under fully denaturing conditions: application in ubiquitin profiling and protein complex identification combined with in vivocross-linking. Mol Cell Proteomics, 5(4), 737-748.

Teis, D., Wunderlich, W., & Huber, L. A. (2002). Localization of the MP1-MAPK scaffold complex to endosomes is mediated by p14 and required for signal transduction. Dev Cell, 3(6), 803-814.

Tyers, M., Rachubinski, R. A., Stewart, M. I., Varrichio, A. M., Shorr, R. G., Haslam, R. J., et al. (1988). Molecular cloning and expression of the major protein kinase C substrate of platelets. Nature, 333(6172), 470-473.

Uetz, P., Giot, L., Cagney, G., Mansfield, T. A., Judson, R. S., Knight, J. R., et al. (2000). A comprehensive analysis of protein-protein interactions in Saccharomyces cerevisiae. Nature, 403(6770), 623-627.

von Mering, C., Krause, R., Snel, B., Cornell, M., Oliver, S. G., Fields, S., et al. (2002). Comparative assessment of large-scale data sets of protein-protein interactions. Nature, 417(6887), 399-403.

Watson, R. T., Kanzaki, M., & Pessin, J. E. (2004). Regulated membrane trafficking of the insulin-responsive glucose transporter 4 in adipocytes. Endocr Rev, 25(2), 177-204.

Watson, R. T., Khan, A. H., Furukawa, M., Hou, J. C., Li, L., Kanzaki, M., et al. (2004). Entry of newly synthesized GLUT4 into the insulin-responsive storage compartment is GGA dependent. EMBO J, 23(10), 2059-2070.

Weghuber, J., Brameshuber, M., Sunzenauer, S., Lehner, M., Paar, C., Haselgrubler, T., et al. (2010). Detection of protein-protein interactions in the live cell plasma membrane by quantifying prey redistribution upon bait micropatterning. Methods Enzymol, 472, 133-151.

Weghuber, J., Sunzenauer, S., Brameshuber, M., Plochberger, B., Hesch, C., & Schutz, G. J. (2010). in-vivo detection of protein-protein interactions on micro-patterned surfaces. J Vis Exp(37).

Weghuber, J., Sunzenauer, S., Plochberger, B., Brameshuber, M., Haselgrubler, T., & Schutz, G. J. (2010). Temporal resolution of protein-protein interactions in the live-cell plasma membrane. Anal Bioanal Chem, 397(8), 3339-3347.

Williams, D., & Pessin, J. E. (2008). Mapping of R-SNARE function at distinct intracellular GLUT4 trafficking steps in adipocytes. J Cell Biol, 180(2), 375-387.

Wu, M., Holowka, D., Craighead, H. G., & Baird, B. (2004). Visualization of plasma membrane compartmentalization with patterned lipid bilayers. Proc Natl Acad Sci U S A, 101(38), 13798-13803.

Xu, Y., Moseley, J. B., Sagot, I., Poy, F., Pellman, D., Goode, B. L., et al. (2004). Crystal structures of a Formin Homology-2 domain reveal a tethered dimer architecture. Cell, 116(5), 711-723.

Yamazaki, T., Zaal, K., Hailey, D., Presley, J., Lippincott-Schwartz, J., & Samelson, L. E. (2002). Role of Grb2 in EGF-stimulated EGFR internalization. J Cell Sci, 115(Pt 9), 1791-1802.

Yasuda, K., Kosugi, A., Hayashi, F., Saitoh, S., Nagafuku, M., Mori, Y., et al. (2000). Serine 6 of Lck tyrosine kinase: a critical site for Lck myristoylation, membrane localization, and function in T lymphocytes. J Immunol, 165(6), 3226-3231.

Zwick, E., Bange, J., & Ullrich, A. (2001). Receptor tyrosine kinase signalling as a target for cancer intervention strategies. Endocr Relat Cancer, 8(3), 161-173.